NMDA RECEPTOR MRNA EXPRESSION IN AUDITORY BRAINSTEM

POSTNATAL DEVELOPMENTAL DISTRIBUTION OF NMDA RECEPTOR SUBUNIT MRNA IN AUDITORY BRAINSTEM OF RAT

By:

ENAKSHI SINGH, H. BSC

A Thesis

Submitted to the School of Graduate Studies in Partial Fulfillment of the Requirements for the Degree Master of Science

McMaster University

MASTER OF SCIENCE (2011) MCMASTER UNIVERSITY

(Neuroscience) Hamilton, Ontario, Canada

TITLE: POSTNATAL DEVELOPMENTAL DISTRIBUTION OF NMDA RECEPTOR SUBUNIT MRNA IN AUDITORY BRAINSTEM OF RAT

AUTHOR: Enakshi Singh, H.BSc (McMaster University)

SUPERVISOR: Dr. Deda C. Gillespie

NUMBER OF PAGES: xii, 97

ABSTRACT

The superior olivary complex (SOC) is comprised of nuclei involved in sound localization. To compute interaural sound level differences, lateral superior olive (LSO) neurons integrate converging glutamatergic inputs from the cochlear nucleus with glycinergic inputs from the medial nucleus of the trapezoid body (MNTB). To compute interaural timing differences, the medial superior olive (MSO) integrates converging glutamatergic inputs from the ipsilateral and contralateral cochlear nucleus. The MSO also receives a major inhibitory input from the MNTB. N-methyl-D-aspartate receptors (NMDARs) are thought to play a role in the developmental refinement of these auditory brainstem pathways. The GluN2A and GluN2B NMDAR subunits confer widely different properties on NMDARs, substantially affecting plasticity. We assessed postnatal developmental messenger RNA (mRNA) expression of GluN1, GluN2A and GluN2B subunits in the LSO, MSO and MNTB using quantitative *in-situ* hybridization in tissue from 10 litters, ages postnatal day 1 to 36 (P1-36).

GluN1 mRNA expression in the LSO, MSO and MNTB decreased with age. In all three nuclei, GluN2B mRNA expression was highest during the first postnatal week, dropping to low levels thereafter. In the LSO, GluN2A levels increased, then decreased to moderate levels. In the MNTB, GluN2A levels decreased from initially high levels. In the MSO, GluN2A levels increased to intermediate levels. The GluN2A/2B ratio increased 2-fold between P1 and P8 in

the MNTB, whereas the ratio increased 3-fold between P8 and P15 in the LSO and MSO. The changes in GluN2A:GluN2B ratio are consistent with a developmental switch from GluN2B-containing NMDARs to GluN2A-containing NMDARs. These results are consistent with prior electrophysiological experiments that show NMDAR-mediated currents declining with age in the aVCN-MNTB, aVCN-LSO and MNTB-LSO pathways. The GluN2A subunit exhibited different developmental expression patterns in MNTB, LSO and MNTB, which suggests that GluN2A mRNA expression is locally regulated between nuclei, whereas GluN2B may be globally regulated.

ACKNOWLEDGEMENTS

The completion of this thesis would not have been possible without the help and support of several people. Most importantly, I am extremely grateful to my supervisor and mentor, Dr. Deda Gillespie for always being there for me. I would also like to thank Dr. Jane Foster, for welcoming me into her lab and treating me as one of her students. I would not have been able to complete all my research required for this thesis without Dr. Fosters' time, guidance, encouragement and support. In addition, I would like to thank all members of the Foster lab, with a special thanks to Aysah Amath and Kelly Rilett for training me and for always being available when I needed help with lab techniques. I also wish to thank all members of the Gillespie lab, especially Alan Cooper, for his support and advice. Alan was always available to answer my questions and I am very grateful for his assistance. I would like to thank my parents for always bringing me home-cooked meals when I needed it most, and my friends for always supporting and encouraging me throughout this journey. Lastly, I would like to thank my committee members for their guidance and assistance.

TABLE OF CONTENTS

LIST OF FIGURES

LIST OF TABLES

LIST OF ABBREVIATIONS AND SYMBOLS

AMPA	∝-amino-3-hydroxy-5-methyl-4-isoxazolepropionic acid
AMPAR	AMPA receptor
aVCN	anteroventral cochlear nucleus
bp	base pairs
cDNA	complementary DNA
CN	cochlear nucleus
CNS	central nervous system
CPM	counts per minute
DCN	dorsal cochlear nucleus
DNA	deoxyribonucleic acid
DPM	disintegrations per minute
GABA	γ-aminobutyric acid
eIPSP	evoked IPSP
EPSC	excitatory post-synaptic current
ER	endoplasmic reticulum
Ex	embryonic day x
ILD	interaural level difference
IPSC	inhibitory post-synaptic current
IPSP	inhibitory post-synaptic potential
ITD	interaural timing difference
KO	knockout

LNTB	lateral nucleus of the trapezoid body
LSO	lateral superior olive
LTD	long-term depression
LTP	long-term potentiation
mIPSC	miniature IPSC
MNTB	medial nucleus of the trapezoid body
mRNA	messenger RNA
MSO	medial superior olive
NM	nucleus magnocellularis
NMDA	N-methyl-D-aspartate
NMDAR	NMDA receptor
PBS	phosphate buffer solution
PCR	polymerase chain reaction
Px	Postnatal day x
pVCN	posteroventral cochlear nucleus
ROI	region of interest
RNA	ribonucleic acid
SEM	standard error of the mean
SOC	superior olivary complex
TEA	triethanolamine
VCN	ventral cochlear nucleus
VGLUT	vesicular glutamate transporter

DECLARATION OF ACADEMIC ACHIEVEMENT

I sectioned all of the brains used in this research project, and performed the subsequent *in-situ* hybridizations on these sections. I also analyzed the digitized *in-situ* images. Dan Case and Dr. Javier Alamilla, from Dr. Deda Gillespie's lab, collected the rat brains and Dr. Jane Foster was involved in the creation of the riboprobes used for the *in-situ* experiments for this project.

1. Introduction

Auditory Brainstem

The ability to accurately and efficiently localize sound relies on the precise synaptic circuitry present within the auditory brainstem. The superior olivary complex (SOC) is composed of nuclei involved in determining the location of a sound source. Sound first enters the ear and is transduced into electrical energy by hair cells in the cochlea. Cochlear hair cells are connected to the brain by spiral ganglion neurons that form the auditory nerve. The auditory nerve innervates three subdivisions of the cochlear nucleus (CN): the anteroventral (aVCN), posteroventral (pVCN) and dorsal cochlear nucleus (DCN).

The SOC contains nuclei involved in the first level of processing of interaural level differences (ILDs) and interaural timing differences (ITDs). Mammals determine the azimuthal location of incoming sound through interaural differences. Interaural timing differences (ITDs) are used to localize a sound source in the horizontal plane, and arise from the difference in the time of arrival of sound to the two ears. Interaural level differences (ILDs) are another cue used to localize sound in the horizontal azimuth, and arise from the difference in sound intensity arriving at two ears. ITD cues are mainly used to determine the location of low frequency sounds, whereas, ILDs are used to determine the horizontal location of high frequency sounds (Caird & Klinke, 1983). The short wavelengths of high frequency sounds are reflected by the head, which creates a sound

shadow large enough to result in interaural intensity differences of sound arriving at the two ears. The long wavelengths of low frequency sounds do not create a large enough shadow to compute intensity differences, and as such, the difference in time of arrival of sound at the two ears is used to localize low frequency sounds.

The three main nuclei within the SOC involved in sound localization are the lateral superior olive (LSO), the medial superior olive (MSO) and the medial nucleus of the trapezoid body (MNTB). Neurons in the MSO are responsible for encoding ITDs (Caird & Klinke, 1983; Goldberg & Brown, 1969) and neurons in the LSO are responsible for computing ILDs (Boudreau and Tsuchitani, 1968, Caird and Klinke, 1983; Sanes & Rubel, 1988). MSO neurons compute ITDs by integrating binaural excitatory inputs from spherical bushy cells of the aVCN and binaural inhibitory inputs from the MNTB and lateral nucleus of the trapezoid body (LNTB), a smaller structure within the SOC (Grothe & Neuweiler, 2000). LSO neurons integrate converging excitatory inputs from spherical bushy cells in the ipsilateral aVCN and inhibitory inputs from the MNTB, driven by the contralateral aVCN, to compute ILDs (see Fig 1 for schematic; Kim & Kandler, 2003; Kotak and Sanes, 1996; Sanes and Rubel, 1988). In the mature system, both excitatory (glutamatergic) and inhibitory (gylcinergic) inputs are tonotopically organized such that a single LSO neuron is excited and inhibited by the same sound frequency (Kotak and Sanes, 1996; Sanes and Rubel, 1988).

Development and refinement of MSO

The MSO principal cells exhibit a bipolar morphology, with two major dendrites extending from the soma, at 180 degrees to each other, and orthogonal with respect to the dorsoventral axis of the MSO (Kapfer et al., 2002). The MSO computes ITDs by integrating binaural excitatory (glutamatergic) inputs from spherical bushy cells of the aVCN (see Fig 1 for schematic; Grothe & Neuweiler, 2000; Kapfer et al., 2002). Excitatory inputs from the ipsilateral aVCN synapse on lateral dendrites and excitatory inputs from the contralateral aVCN synapse on medial dendrites of MSO neurons (Kapfer et al., 2002). The contribution of different glutamate receptors to the excitatory response of MSO neurons is yet to be determined. It was originally thought that ITDs were encoded by coincidence detection of these binaural excitatory inputs; however, bilateral inhibitory inputs from the MNTB and LNTB are also important for the encoding of ITDs (Grothe & Neuweiler, 2000). The bilateral MNTB-MSO projections are primarily glycinergic, and synapse mainly on the soma in the mature MSO (Kapfer et al., 2002).

To examine the developmental changes of glycinergic inputs to the MSO, Magnusson et al. (2005) performed whole-cell patch recordings in principal cells of gerbil MSO between postnatal day 12 to 25 (P12-P25). The inhibitory MNTB or LNTB fibers were stimulated, and inhibitory post-synaptic currents (IPSCs) and inhibitory post-synaptic potentials (IPSPs) were recorded from the MSO. After hearing onset (P12), evoked IPSCs (eIPSCs) developed kinetics that were approximately two times faster than those measured at hearing onset, as

measured by a decrease in the decay time constant. This acceleration of IPSC kinetics mainly occurred between P12 and P17 (Magnusson et al., 2005). To investigate if an increase in release synchrony of transmitter quanta accounted for the acceleration of eIPSCs, Magnusson et al. (2005) isolated spontaneous miniature IPSCs (mIPSCs) and compared mIPSCs to evoked IPSCs (eIPSCs). Isolated mIPSCs did not exhibit changes in rise time and decay kinetics between P12 and P20, indicating that during this time, there is likely an increase in synchrony of action potential-evoked transmitter release. In addition, the frequency of spontaneous mIPSCs decreased approximately three-fold during this time, providing evidence for a decrease in the number of functional glycinergic synapses. After hearing onset, these authors also saw a four-fold increase in IPSP kinetics, as measured by a significant shortening of IPSP half-width and rise time. A decrease in input resistance was also seen between P12 and P20; thus, the acceleration of IPSP kinetics is likely a result of a decrease in input resistance (Magnusson et al., 2005). Gerbils reared in omni-directional noise did not exhibit these activity-dependant changes seen in glycinergic inputs to the MSO (Magnusson et al., 2005). Therefore, these results provide evidence that functional refinement, as measured by electrophysiological techniques, occurs after hearing onset and is likely dependent on synaptic activity. Werthat et al. (2008) visualized developmental changes in axonal arborisation of MNTB-MSO connections during the first two weeks post hearing onset. Individual MNTB-MSO axonal arbors were visualized by Microruby tracer injection in the

MNTB. During the two postnatal weeks after hearing onset, Werthat et al. (2008) observed a significant reduction in the number of branch points and axon endsegments. The refinement of inputs occurred along the dorso-ventral axis, and from a somato-dendritic location to a mostly somatic location on individual MSO neurons (Werthat et al., 2008). To examine the morphology of MSO neurons, Rautenberg et al. (2009) labeled MSO neurons with fluorescent dyes by single-cell electroporation. Serial optical sections of fluorescently labeled cells were taken at a confocal microscope and reconstructed in three-dimensions by compartmentalization (Rautenberg et al., 2009). These authors quantified the morphological changes of MSO neurons, in gerbils, between P9 and P36. Between P9 and P21, the number of branch points decreased, and this decrease was accompanied by a reduction in total length and surface area of the cell. In addition, the cell volume increased until P27, which coincided with a two-fold increase in dendritic diameter. Morphological refinement of the MSO was thus complete by P27 (Rautenberg et al., 2009). These functional and structural changes occurred after hearing onset and therefore are likely dependent on auditory experience. In addition, the restriction of inhibitory inputs to the somata of MSO neurons coincides with the refinement that occurs in the two postnatal weeks after hearing onset.

Development and refinement of aVCN-LSO pathway

The tonotopic organization of the aVCN-LSO pathway is present before the onset of synaptic activity (Jackson & Parks, 1982; Molea & Rubel, 2003). Whether synapse elimination and axonal pruning of auditory nerve fibers occurs in the CN has been difficult to determine in mammals. In the avian analog of the ventral CN, the nucleus magnocellularis (NM), auditory nerve axons begin to form synapses around embryonic day 11 to 13 (E11-13) (Jackson & Parks, 1982). These synapses are functional, as synaptic transmission in NM neurons is also present at E12 (Jackson & Parks, 1982; Lu & Trussell, 2007). Jackson & Parks (1982) examined the development of the NM using both electrophysiological and anatomical methods. Jackson & Parks (1982) recorded responses to stimuli of increasing amplitude, and then plotted input-output curves of response amplitude as a function of stimulus amplitude for each neuron. By using this technique, these authors determined the number of auditory nerve axons innervating a single NM neuron. The mean number of discrete steps decreased from 4.0 at E13 to 2.2 at E17-18, thus, the number of fibers innervating a single NM neuron decreased during this time. In addition, for their anatomical studies, NM neurons were labeled with horseradish peroxidase in order to examine the morphological changes throughout development. At E14, most auditory nerve axons exhibited terminal branching on NM neurons. By E17/18, one or two auditory nerve fibers had formed the large and powerful synapse terminals, the endbulbs of Held, on the soma of NM neurons (Jackson & Parks, 1982). In summary, a 50% decrease

in the number of cochlear nerve axons innervating individual NM neurons was seen between E13 and E17/18 (Jackson & Parks, 1982).

Using electrophysiology, Lu & Trussell (2007) examined synaptic transmission mediated by ∝-amino-3-hydroxy-5-methyl-4-isoxazolepropionic acid (AMPA) and N-methyl-D-aspartate (NMDA) glutamate receptors in NM neurons of the chick, between E12 and E19. They found that weakening of synaptic connections, as measured by a decrease in AMPA receptor-mediated quantal size, preceded synapse elimination. Furthermore, those synaptic terminals that were maintained were strengthened by an increase in AMPA receptor-mediated quantal size (Lu & Trussell, 2007). Between E12 and E19, the contribution of AMPA receptor-mediated excitatory post-synatpic currents (EPSCs) increased by approximately 30%, whereas NMDA receptor-mediated EPSCs peaked at E14 and declined thereafter (Lu & Trussell, 2007). The NMDAR EPSC decay time remained relatively constant during the ages examined. The decay time of NMDAR-mediated EPSCs varied with subunit composition of the NMDAR (refer to section on NMDARs for more information). NMDARs containing the GluN2B subunit are thought to be the predominant form of NMDA receptors in the NM. As will be discussed in a later section, the subunit composition of NMDARs is dynamic, and changes with development in many sensory areas (Carmignoto & Vicini, 1992; Crair & Malenka, 1995; Flint et al., 2007; Hestrin, 1992; Takahashi et al., 1996). Subunit-specific pharmacology provided no evidence for a switch in

NMDAR subunit composition throughout development of the NM (Lu & Trussell, 2007).

Leake et al. (2002) used anatomical tracing to examine the topographic organization of the auditory nerve projections to the CN during early postnatal development in the cat. Auditory nerve projections to all three subdivisions of the CN demonstrate a tonotopic organization, as defined by distinct isofrequency bands (Leake et al., 2002). The size of the CN subdivisions and the width of the isofrequency bands both increase with age, but the increase in the size of the CN is greater than the increase in the width of the isofrequency bands during the first postnatal week. As a result, the relative width of the isofrequency bands becomes smaller during this time. So, in the cat, topographic sharpening is accomplished by an increase in the size of the CN complex (Leake et al., 2002). Because this refinement is complete prior to hearing onset, it is likely independent of auditory experience.

Synaptic transmission in the VCN-LSO pathway has been examined using whole-cell voltage clamp in brainstem slices from rats postnatal day 1 to 12 (P1-12) (Case et al., 2011). Synapse elimination at VCN-LSO synapses occurred between P3/4 and P8/9. Between P1 and P3, all LSO neurons received greater than three VCN inputs, whereas, at P9-12, most LSO neurons received less than three VCN inputs (Case et al., 2011). Additional strengthening of maintained VCN-LSO synapses continued after P8/9 till hearing onset at P12. Synapse elimination was accompanied by an increase in the fractional contribution of

AMPAR-mediated EPSCs and a decrease in the fractional contribution of NMDAR-mediated EPSCs (Case et al., 2011). The decay time and mean charge transfer of NMDAR-mediated EPSCs decreased substantially between birth and hearing onset (Case et al., 2011). Using subunit specific pharmacology, Case et al. (2011) found evidence for high levels of GluN2B-containing NMDA receptors in the first postnatal week, specifically between P3 and P9. These experiments support the notion that even though there is a tonotopic organization in the VCN-LSO pathway connections at birth, connections are further refined after birth, mainly by synapse elimination and strengthening of the maintained synapses.

Development and refinement of aVCN-MNTB-LSO pathway

Axonal outgrowth of both the excitatory and inhibitory connections in the aVCN-MNTB-LSO pathway begins at E18 (Kandler & Friauf, 1993). These connections are functional, as in the LSO, ipsilateral and contralateral synaptic transmission is present at E18 (Kandler & Friauf, 1995). The excitatory and inhibitory frequency tuning curves of most LSO neurons are aligned by the time of hearing onset. Thus, auditory experience is not necessary for the majority of the refinement of the MNTB-LSO pathway (Sanes & Rubel, 1988). However, patterned spontaneous activity from the cochlea, beginning at around P3, is thought to be important for the refinement of this pathway (Sanes & Takacs, 1993; Tritsch et al., 2007; Tritsch & Bergles, 2010). Topographic precision is accomplished by early functional refinement, that occurs prior to hearing onset

(Kim & Kandler 2003; Kim & Kandler, 2010) and a later structural refinement, which occurs after hearing onset (Rietzel & Friauf, 19998; Sanes & Friauf, 2000).

aVCN-MNTB pathway

Globular bushy cells in the aVCN project onto principal neurons of the contralateral MNTB (see Fig 1; Smith et al., 1991). This giant synapse is referred to as the calyx of Held, and is the largest excitatory synapse in the CNS (Smith et al., 1991). The calyx of Held forms early in development, with projections from the aVCN seen by E15 (Kandler & Friauf, 1993). By P3, the calyx of Held synapse appears to be fully formed (Kandler & Friauf, 1993; Rodriguez-Contreras et al., 2008). The inputs from the aVCN to the MNTB are primarily glutamatergic, and form a one-to-one connection between the aVCN and the MNTB (Smith et al., 1991; Joshi & Wang, 2002; Steinert et al., 2010). Joshi & Wang (2002) performed whole-cell recordings from MNTB neurons in slices from mice between P5 and P18. These authors found that evoked EPSCs contained a fast AMPAR-mediated component and a slower NMDAR-mediated component. NMDAR-mediated EPSCs increased until P11/12, then declined to low levels by P16, whereas, AMPAR-mediated EPSCs increased in amplitude by approximately three-fold (for a more in-depth review, refer to “Glutamate receptors in auditory brainstem” section; Joshi & Wang, 2002).

MNTB-LSO pathway

Kim & Kandler (2003) performed whole-cell recordings in the LSO in brainstem slices from rats. While recording in the LSO, the MNTB was stimulated using focal photolysis of caged glutamate. These authors stimulated the MNTB from 80 – 120 locations spaced ~50 μm, then mapped individual MNTB-LSO connections between P1 and P14. In neonatal rats (P1-4), individual LSO neurons received synaptic inputs from approximately 36% of the MNTB cross-sectional area. In older rats, around the time of hearing onset (P11-14), individual LSO neurons received synaptic inputs from approximately 8% of the MNTB cross-sectional area. The input area of the MNTB decreased by approximately 75% during the first two postnatal weeks. These authors also compared the width of the input maps, as the tonotopic gradient of the MNTB is seen along the mediolateral axis of the MNTB. By comparing the input width of neonatal rats to older rats, Kim & Kandler (2003) were able to quantify the sharpening of MNTB-LSO connections along the tonotopic axis. Input width decreased by approximately 50%, and this decrease was seen during the first postnatal week, mainly from P3 to P8 (Kim & Kandler, 2003). Thus, the restriction of input maps with development resulted in approximately a two-fold increase in topographic precision. In addition, those MNTB-LSO connections that were maintained were strengthened, as seen by an increase in quantal size and quantal content (Kim & Kandler, 2003; Kim & Kandler, 2010). As previously mentioned, synaptic strengthening of maintained VCN-LSO synapses continues beyond P8 in the

VCN-LSO pathway (Case et al., 2011), and this additional strengthening hasn't been reported in the MNTB-LSO pathway. Functional refinement of the MNTB-LSO pathway is followed by a period of anatomical refinement during which the axons and dendrites of the MNTB-LSO pathway become restricted tonotopically (Rietzel & Friauf, 1998; Sanes & Takacs, 1993). Anatomical refinement occurs after hearing onset, and thus is likely dependent on auditory experience (Sanes & Takacs, 1993). Because there is a delay between functional refinement and anatomical refinement, an interesting question is whether there are different mechanisms guiding the two distinct periods of refinement.

During the period of functional refinement (prior to hearing onset), inhibitory neurotransmitters, GABA and glycine, released at nascent MNTB-LSO synapses exert a depolarizing action (Ehrlich et al., 1999; Kandler & Friauf, 1995). This is because the high intracellular chloride concentration ($[Cl^-]_i$) sets the chloride reversal potential in immature LSO neurons as more positive than the resting membrane potential (Ehlrich et al., 1999; Kakazu et al., 1999). The mechanisms that account for the high $[Cl^-]_i$ in immature LSO neurons are not completely understood; however, it is known that, in mature LSO neurons, the potassium (K+) chloride (Cl^-) cotransporter KCC2 is responsible for maintaining the low $[Cl^-]_i$ concentration (Balakrishnan et al., 2003). In many other areas of the brain, the sodium potassium chloride (Na^+ K^+ $2Cl^-$) cotransporter, NKCC1, is responsible for maintaining the high $[Cl^-]_i$ concentration at younger ages (Balakrishnan et al., 2003; Becker et al., 2003). NKCC1 is not expressed in

immature LSO neurons (Balakrishnan et al., 2003), but the $HC03^-/Cl^-$ exchanger, AE3, is thought to play a role in maintaining the high $[Cl^-]_I$ in the immature LSO (Becker et al., 2003). Thus, the balance of AE3 and KCC2 expression is likely responsible for the change in the chloride reversal potential seen with development. The depolarizing effect of GABA and glycine on immature LSO neurons results in chloride efflux through postsynaptic GABA and glycine receptors, inducing action potentials in the LSO (Kullman et al., 2002). Depolarizing GABA and glycine input opens voltage-gated calcium channels. Calcium influx through voltage gated calcium channels can result in the initiation of calcium-dependent intracellular signaling cascades, which are thought to be important in the development and refinement of this pathway (Kotak & Sanes, 2000; Lohman et al., 2007).

MNTB terminals also shift from being both GABAergic/glycinergic to being primarily glycinergic by the time of hearing onset (Kotak & Sanes, 1998; Nabekura et al., 2004). GABA, but not glycine, can induce long-term depression of MNTB-LSO synapses (Chang et al., 2003; Kotak & Sanes, 2000). In addition, GABA-mediated IPSCs exhibit a longer decay time than glycine-mediated IPSCs, thus allowing for more Ca2+ entry (Nabekura et al., 2004). Both GABA release and calcium influx have been shown to be important for long-term depression (LTD) of LSO neurons (Kotak & Sanes, 2000). LTD often precedes synapse elimination, therefore, the transient GABAergic phenotype may be important for the refinement of this pathway (Kotak & Sanes, 2000).

During the first postnatal week, the MNTB also releases the excitatory neurotransmitter glutamate (Gillespie et al., 2005). The MNTB transiently releases glutamate during the period when GABA/glycine are also depolarizing. As such, depolarizing GABA/glycine can relieve the magnesium block of NMDA receptors (NMDARs) (for more information on properties of NMDARs, refer to the 'NMDA Receptors' section), thus allowing glutamate to activate postsynaptic NMDARs (Gillespie et al., 2005). Because of the importance of NMDA receptors in many forms of developmental plasticity (Barria & Malinow, 2005; Crair & Malenka, 1995; Caroll & Zukin, 2002; Cull-Candy et al., 2005; Philpot et al., 2001) glutamate release and subsequent activation of postsynaptic NMDA receptors may mediate developmental plasticity in the MNTB-LSO pathway. In support of this hypothesis, mice lacking glutamate co-transmission exhibited impaired refinement of the MNTB-LSO pathway (Noh et al., 2010). Using vesicular glutamate transporter 3 (VGLUT3) knockout mice, Noh et al (2010) examined the refinement of the MNTB-LSO pathway compared to control mice. Because VGLUT3 is the primary vesicular glutamate transporter expressed in immature MNTB terminals (Gillespie et al., 2005), VGLUT3 knockout (KO) mice exhibit impaired glutamate co-transmission. VGLUT3 KO mice also exhibited an impaired refinement of the MNTB-LSO pathway, and a less precise tonotopic organization (Noh et al., 2010).

NMDA Receptors

The release of glutamate from presynaptic terminals activates ionotropic and metabotropic glutamate receptors. Ionotropic glutamate receptors include NMDA, AMPA and kainate receptors. The following section focuses primarily on NMDARs, which are important mediators of excitatory synaptic transmission in all areas of the brain. At resting membrane potential, the pore of the NMDA receptor is typically blocked by a magnesium ion (Mg^{2+}). In order for NMDA receptors to be activated, glutamate must be released and the postsynaptic cell must be depolarized to relieve the Mg^{2+} block (Monyer et al., 1994). Under the hypothesis that glutamate release is important for the refinement of the MNTB-LSO connections, the depolarizing effect of GABA/glycine on immature LSO neurons could remove the Mg^{2+} block, and glutamate release could subsequently activate NMDA receptors.

NMDARs mostly exist as heterodimers composed of two GluN1 subunits and two subunits that can be GluN2A - D or GluN3A – B (Cull-Candy et al., 2001; Monyer et al., 1992; Rosenmund et al, 1998). NMDA receptors can also exist as heterotrimers containing two GluN1 subunits and two different GluN2/GluN3 subunits (Cull-Candy et al., 2001; Cull-Candy et al., 2004). Every functional NMDAR must contain two GluN1 subunits, and as such, GluN1 is an obligatory subunit of NMDARs (Ishii et al., 1993; Cull-Candy et al., 2001). GluN1 subunits assemble with GluN2/3 subunits in the endoplasmic reticulum (ER) to form

functional NMDAR channels (Caroll & Zukin, 2002; Cull-Candy et al., 2004; Okabe et al., 1999).

Subunit composition

The subunit composition of a NMDAR influences its physiological properties, including decay time, EPSC amplitude, opening probability, calcium permeability, and voltage sensitivity (Monyer et al., 1994). The GluN3 subunit, when combined with GluN1/GluN2, reduces calcium permeability and thus current flow, and can also influence surface expression (Cull-Candy et al., 2004). NMDARs composed of GluN1/GluN3A or –3B subunits are selectively activated by glycine, are resistant to magnesium block, impermeable to calcium, and unaffected by glutamate, NMDA or NMDAR antagonists (Cull-Candy et al., 2004). The GluN2 subunits confer a wide range of decay time constants. GluN2A-containing NMDARs exhibit a decay time constant that is approximately 3-4 times faster than GluN2B and GluN2C-containing NMDARs (Monyer et al., 1994; Banke & Traynelis, 2003). GluN2D-containing NMDARs exhibit a decay time constant that is between 10 and 40 times longer than the decay time constants of the other subunits (Monyer et al., 1994). NMDARs containing GluN2A exhibit smaller EPSCs when compared to GluN2B-containing NMDARs (Barria and Malinow, 2002). Although GluN1/GluN2B-containing NMDARs have lower opening probabilities, once open, the receptors deactivate at a much slower rate (Erreger et al., 2005). All NMDARs exhibit high calcium permeability, but GluN2B-

containing NMDARs carry more calcium per unit of current than GluN2A-containing NMDARs (Sobczyk et al., 2005). In one very well known version of hippocampal LTP, calcium entering through NMDARs binds to the calcium-binding protein, calmodulin (Strack & Colbran, 1998). The calcium-calmodulin complex then activates CaMKII, which is important for the induction of NMDAR-dependent LTP (Barria & Malinow, 2005). Activated CaMKII binds to the GluN2B subunit with a greater affinity than GluN2A (Barria & Malinow, 2005). The voltage sensitivity of the magnesium block also varies between GluN2 subunits. GluN2A-containing and GluN2B-containing NMDARs exhibit a stronger voltage sensitivity of the magnesium block than GluN2C-containing and GluN2D-containing NMDARs (Monyer et al., 1994). Subunit-specific pharmacology can be used to determine subunit composition of NMDARs. NMDA currents induced at GluN1/GluN2B receptors are inhibited by ifenprodil with high affinity (Williams, K., 1993). Ifenprodil exhibits a lower affinity for GluN1/GluN2A receptors when compared to GluN1/GluN2B NMDARs, and as such, ifenprodil is used to distinguish between subunit types in the brain. Ro-25 6891 is another GluN2B-specific antagonist that can be used to block GluN2B-containing NMDARs (Liu et al., 2004); however, the action of ifenprodil, Ro-25 6981 and similar antagonists on triheteromeric NMDA receptors is currently unknown (Cull-Candy et al., 2004). In many sensory areas, the amount of inhibition of NMDAR-mediated excitatory postsynaptic currents (EPSCs) by ifenprodil decreases with development (Joshi & Wang, 2002; Cull-Candy et al., 2004). This change in ifenprodil sensitivity is

attributed to a change in NMDA receptor composition, specifically a decrease in GluN2B-containing NMDA receptors.

NMDA receptor assembly and trafficking

The GluN1 subunit is thought to play a major role in controlling the delivery of NMDA receptors to the synapse (Okabe et al., 1999; Caroll & Zukin, 1999; Cull-Candy et al., 2004). The GluN1 subunit exists in eight functional isoforms, all formed by combinations of three independent splice variants from the same gene (Cull-Candy et al., 2004). GluN1 splice variants with short C-terminal tails (GluN1-4a and GluN1-4b) are mostly seen at the surface of the cell, whereas splice variants with long C-terminal tails (GluN1-1a and GluN1-1b) are mostly retained within the cell (Carroll & Zukin, 2002; Okabe et al., 1999). The C-terminal tail of GluN1 subunits is thus important for the exit of NMDARs from the ER to the cell surface (Caroll & Zukin, 2002; Okabe et al., 1999). There may be signals within the C-terminus of the GluN1 subunit that keep unassembled NMDARs within the ER. The splice cassette, C1, has been shown to contain an ER retention/retrieval motif (Cao et al., 2011). This ER retention motif is shielded by GluN1 subunits assembling with GluN2/3 subunits, thus allowing for assembled NMDARs to leave the ER (Cao et al., 2011). In addition, a PDZ binding domain, in GluN1 splice variants containing the C2 cassette (GluN1-3a and GluN1-3b) (Okabe et al., 1999), also promotes the exit of assembled NMDARs from the ER. The PDZ binding domain may block the ER retention

signal or PSD-95 may bind to the PDZ binding domain and thus blocking the ER retention signal (Carroll & Zukin, 2002). Protein kinases are also known to play a role in synaptic transmission of NMDARs. Phosphorylation of serine at position 896 (Ser896) by protein kinase C and Ser897 by cAMP-dependent protein kinase, which are closely located to the ER retention motif, may also promote the exit of newly assembled NMDARs from the ER (Carrol & Zukin, 2002). The GluN1 subunit is therefore essential for exit of NMDARs from the ER.

Expression Patterns of NMDA Receptors in the Brain

The NMDAR subunits exhibit different expression patterns throughout the brain and the subunit composition of NMDARs changes with development. Expression levels of the obligatory GluN1 subunit remain relatively constant in all brain areas (Monyer et al., 1992; Ishii et al., 1993). The GluN2B-containing NMDARs are most prevalent at embryonic stages, with GluN2B messenger RNA (mRNA) most predominantly expressed in the forebrain (Ishii et al., 1993), whereas GluN2D mRNA is most prevalent in the diencephalon and brainstem (Ishii et al., 1993; Cull-Candy et al., 2001). GluN2A-containing NMDARs are detectable shortly after birth, and GluN2A mRNA is mainly expressed in the cerebral cortex and hippocampus (Ishii et al., 1993). GluN2C mRNA is mostly seen in the cerebellum (Cull-Candy et al., 2001).

Role of NMDA receptors in plasticity

NMDAR EPSCs are generally longer at younger ages when compared to EPSCs in adulthood in the rat visual cortex (Carmignoto & Vicini, 1992), rat somatosensory cortex (Crair & Malenka, 1995; Flint et al., 2007), rat superior colliculus (Hestrin, 1992) and mouse cerebellum (Takahashi et al., 1996). The change in decay time of EPSCs, usually attributed to a switch from GluN2B to GluN2A, is thought to coincide with the end of critical periods for synaptic plasticity in the developing brain (Crair & Malenka, 1995; Flint et al., 2007; Hestrin, 1992). In support of this hypothesis, rats reared in complete darkness show a delay in the developmental decrease of NMDAR-mediated EPSCs (Carmignoto & Vicini, 1992). The ratio of GluN2A/GluN2B-containing NMDARs has also been found to increase with development (Hestrin et al., 1992; Monyer et al., 1994; Sheng et al., 1994; Flint et al., 1997; Yoshimura et al., 2003). Since GluN2B-containing NMDARs exhibit a longer decay time than GluN2A-containing NMDARs (Banke & Traynelis, 2003; Barria and Malinow, 2002; Monyer et al., 1994), the increase in the ratio of GluN2A to GluN2B with age accounts for the decrease in decay time also seen with age.

NMDA receptors may be involved in metaplasticity, a change in the threshold required to induce LTP or LTD (Abraham & Bear, 1996). Sensory deprivation lowers the threshold for LTD induction in the visual cortex of dark-reared animals (Philpot et al., 2003). This effect can be reversed by partial blockade of NMDARs. Light deprivation also decreases the ratio of GluN2A to

GluN2B, whereas light experience increases this ratio (Philpot et al., 2001). The change in NMDAR subunit composition with experience and deprivation may account for the change in the threshold required to induce plasticity in the visual cortex. A high GluN2A/GluN2B ratio may favor LTD induction by limiting calcium entry through NMDARs. In support of this view, GluN2B-containing NMDARs are open longer (Monyer et al., 1994), and carry more calcium per unit of current (Sobczyk et al., 2005). In addition, application of ifenprodil (GluN2B-specific antagonist) prevents LTP in immature hippocampal cultures (Barria & Malinow, 2005). CaMKII is implicated in being involved in NMDAR-dependent LTP, and binds with a higher affinity to GluN2B-containing NMDARs when compared to GluN2A-containing NMDARs (Leonard et al., 1999; Barria & Malinow, 2005). Thus, the subunit composition of NMDARs may influence the direction and threshold for LTP/LTD in immature and mature neuronal connections. Philpot et al. (2007) found that GluN2A knockout mice exhibited similar NMDAR EPSC kinetics as dark-reared wild-type mice. In addition, GluN2A knockouts did not exhibit the same reduction in the threshold required to induce plasticity (Philpot et al., 2007). These results suggest that the ratio of GluN2A/GluN2B-containing NMDARs may be involved in establishing the threshold for activity-dependent synaptic modifications.

It has also been suggested that the different NMDAR subunits may influence the direction of plasticity. Liu et al. (2004) investigated the effect of applying subunit-specific antagonists on the direction of synaptic plasticity.

Blocking GluN2B-containing NMDARs with GluN2B-specific antagonists (ifenprodil and Ro 25-6981 maleate) prevented the induction of LTD by low frequency stimulation. Application of a GluN2A-specific antagonist (NVP-AAM077) blocked the induction of LTP by high frequency stimulation. Liu et al. (2004) suggest that GluN2B-containing NMDARs are important for the induction of LTD whereas GluN2A-containing NMDARs are important for LTP induction. In support of these findings, Zhao & Constantine-Paton (2007) demonstrated that GluN2A knockout mice exhibited impaired LTP, but not LTD induction. In addition, Brigman et al. (2010) generated mice with a late-developmental deletion of GluN2B in the CA1 subregion of the hippocampus and in cortical pyramidal neurons. These mutant mice exhibited faster decaying NMDAR-mediated EPSCs when compared to control mice and did not exhibit LTD with a protocol that did induce LTD in control mice (Brigman et al., 2010). These results suggest that GluN2B-containing NMDARs may be important for the induction of LTD. However, other groups have found contradictory results. Barria and Malinow (2005) suggest that CaMKII binding to GluN2B-containing NMDARs is important for the induction of LTP. Moreover, the specificity of NVP-AAM077 (GluN2A-specific antagonist) in blocking only GluN2A-containing receptors has been questioned (Berberich et al., 2005). Berberich et al. (2005) found that LTP could be induced in the presence of NVP-AAM077, which contradict the results found by Liu et al. (2004). Foster et al. (2010) examined the roles of GluN2A and GluN2B in LTP by using overexpression and RNA interference (RNAi)

knockdown of these subunits in hippocampal slice cultures. LTP was blocked by Ro25-6981 (GluN2B-specific antagonist) at younger ages (days in vitro (DIV) 6-8). However, LTP was not blocked by Ro25-6981 in older slices (DIV 11-14). RNA interference knockdown of GluN2B combined with GluN2A overexpression prevented LTP in older slices (DIV 11 – 14). Foster and colleagues suggest that GluN2B activation at older ages may not be required for LTP induction, but this subunit must be present structurally in order for LTP to be induced. In support of this, Foster et al. (2010) found that an RNAi-resistant GluN2B cytoplasmic tail fused to the N-terminus of GluN2A was sufficient to restore LTP. The reverse construct (GluN2B N-terminus fused to GluN2A C-terminus) did not restore LTP. The cytoplasmic tail of the GluN2B subunit may be important for recruiting molecules important for LTP induction (Barria and Malinow, 2005; Foster et al., 2010). GluN2B and GluN2A-containing NMDARs may actually both contribute to LTP in mature synapses (Foster et al., 2010).

Glutamate Receptors in Auditory Brainstem

AMPA receptors exhibit changes in subunit expression in nuclei of the auditory brainstem during development (Caicedo & Eyebalin, 1999). AMPA receptors are hetero-oligomers (containing five subunits) of different combinations of the four subunits GluR1, GluR2, GluR3 and GluR4. Caicedo & Eyebalin (1999) used immunohistochemistry to examine the developmental expression of AMPA receptor subunits in the auditory brainstem. In the cochlear

nucleus complex, GluR2, GluR3 and GluR4 neuronal staining was widespread and increased in intensity during development; however, in the SOC, GluR1 and GluR2 subunits predominate at early ages, followed by a progressive increase of GluR4-containing AMPARs (Caicedo & Eyebalin, 1999). Thus, it appears that GluR1/GluR2-containing AMPARs predominate in the SOC prior to hearing onset. After hearing onset, GluR4-containing NMDARs predominate in the SOC.

Caicedo & Eyebalin (1999) also examined the developmental expression of NMDAR subunits, GluN1 and GluN2A/B, in the SOC. Immunostaining for the GluN1 subunit was moderate to intense throughout the CN and SOC starting at P4, and remaining relatively constant during development. At P4, GluN2A/B staining was widespread throughout all areas of the auditory brainstem. By adulthood, staining intensity of GluN2A/B subunits was higher in the CN, LSO, MSO, and superior periolivary nucleus (SPN) when compared to other regions of the auditory brainstem (Caicedo & Eyebalin, 1999).

Hsieh et al. (2002) determined expression patterns of GluN2A and GluN2B mRNA in rat auditory cortex and thalamus from P4 to adulthood. GluN2B mRNA levels were initially high and remained high, with a slight decline in adulthood. GluN2A mRNA levels were initially low, but increased until about P18 before decreasing slightly (Hsieh et al., 2002). Sato et al. (1999) used in non-radioactive and radioactive *in situ* hybridization and immunocytochemistry to determine the subunit composition of NMDA receptors in mature rat SOC. GluN1 expression was highest in all major regions of the SOC. The LSO had high GluN2A and

GluN2C expression, but low GluN2B expression. The MNTB had higher GluN2B than GluN2A and GluN2C. Lastly, the MSO had relatively equivalent expression patterns of GLN2A, -2B, and -2C. GluN2D expression was the lowest in all areas of the SOC (Sato et al., 1999).

Functional studies, using whole-cell physiology and subunit-specific pharmacology, have provided evidence for high levels of GluN2B-containing NMDARs in the LSO in the first postnatal week (Case et al., 2011; Case & Gillespie, 2011). The contribution of NMDARs to EPSCs was highest between P3 and P9 (Case & Gillespie, 2011). The decay time of NMDAR-mediated EPSCs decreased after P9, suggesting that there may be a switch in NMDAR subunit composition (Case & Gillespie, 2011). In addition, application of ifenprodil resulted in a decrease in charge transfer and peak current amplitude. Case & Gillespie (2011) suggest that GluN2B-containing NMDARs are expressed during the first postnatal week, which accounts for the large charge transfer seen during this time. Joshi & Wang (2002) characterized the developmental changes in synaptic responses in mice by performing whole-cell recordings from pre- and postsynaptic terminals in the MNTB. NMDA receptor-mediated EPSCs increased until P11/12, declining to low levels by P16 (Joshi & Wang, 2002). The decay time constant of NMDAR-mediated EPSCs also decreased by about 30% during this time. Subunit-specific pharmacology did not provide strong evidence for a switch in subunit composition (Joshi & Wang, 2002), which suggests that both GluN2A and GluN2B subunits are present across development. The presence of

triheteromeric NMDA receptors could account for the difficulty in using subunit-specific reagents to determine subunit composition (Joshi & Wang, 2002). Physiology techniques are hard to administer at mature brainstem synapses, and as such, few groups have examined NMDAR-mediated EPSCs from the MNTB. Steinert et al. (2010) performed whole-cell patch recordings from MNTB neurons in rats and mice at physiological temperatures and examined NMDAR-mediated responses from P11 (around hearing onset) to adult. The NMDAR-mediated EPSC amplitude decreases and decay time constants decrease with age, reaching stable levels at around P18 (Steinert et al., 2010). The faster kinetics seen at P18, and older ages, is attributed to GluN2A-containing NMDA receptors (Steinert et al., 2010). In addition, a reduction in Mg2+ sensitivity was also seen from P11 to P18. Steinert et al. (2010) attribute this change in magnesium sensitivity to an increased expression of GluN2C-containing NMDA receptors. So, there is a decrease in GluNB-containing channels upon hearing onset, followed by an increase in GluN2A and GluN2C-containing NMDA receptors (Steinert et al., 2010). Joshi & Wang (2002) found that NMDAR-mediated EPSCs virtually disappear in MNTB neurons after P16, whereas Steinert et al. (2010) show that NMDAR-mediated responses are still present at mature ages. As mentioned, Steinert and colleagues (2010) made their recordings at physiological temperatures, whereas Joshi & Wang (2002) recorded at room temperature. The presence of NMDAR-mediated EPSCs at mature ages (after P16) suggests that NMDA receptors are functionally present long after synaptic refinement is

complete. Steinert et al. (201) suggest that NMDA receptors in the mature MNTB are heterotrimers consisting of GluN1, -2A and -2B subunits. However, the developmental expression patterns of NMDA receptor subunits within the MNTB-LSO pathway are currently unknown.

Summary

The three main nuclei of the SOC are the LSO, MSO and MNTB. The LSO computes ITDs by integrating converging glutamatergic inputs from the aVCN and glycinergic inputs from the MNTB. The MSO computes ITDs by integrating glutamatergic inputs from the two aVCNs, and the glycinergic input from the MNTB is important for fine-tuning of the ITDs. These computations require a precise tonotopic organization. Electrophysiological studies have found functional evidence for high levels of GluN2B-containing NMDARs in the aVCN-LSO and MNTB-LSO pathways. In addition, impaired glutamate co-transmission results in a less precise tonotopic organization in the MNTB-LSO pathway. This supports the hypothesis that NMDARs play a role in the developmental refinement of the pathways within the SOC. The NMDAR consists of two obligatory GluN1 subunits combined with one or two GluN2 (A – D) or GluN3 (A – B) subunits. The different NMDAR subunits confer different physiological properties on to the NMDAR. The GluN2A and GluN2B subunits have been implicated in different forms of plasticity. The developmental expression patterns of NMDAR subunits in the auditory brainstem are currently unknown.

Objective

The objective of this study was to examine the mRNA expression of NMDA receptor subunits, GluN1, GluN2A and GluN2B throughout development in the auditory brainstem of rats. Specifically, we wanted to examine the expression patterns of these subunits in the LSO, MSO and MNTB during the first five postnatal weeks of development.

Hypothesis

Based on NMDAR receptor subunit expression patterns in other sensory areas, we expect to see high GluN2B expression at younger ages of development. In addition, we expect to see the GluN2A subunit expressed at higher levels at older ages. Because the ratio of GluN2A to GluN2B increases with development in other sensory areas, we expected to see a similar trend in all three auditory brainstem nuclei examined.

2. Methods

Animals

Ten litters of Sprague-Dawley rats, at P1 – 36 were used in this study. Rat pups were born on site to dams bred on site or purchased pregnant from Charles River Laboratories. Pups were housed with their mothers until weaning at postnatal day 22, and all animals were housed on a normal light/dark cycle (lights off at 7pm and on at 7am). All procedures involving animals were performed in

accordance with Canadian Council on Animal Care guidelines, and were previously approved by the Animal Review Ethics Board of McMaster University.

Tissue collection

Rats of six postnatal days (1, 8, 15, 22, 28 and 36) were euthanized by decapitation. Ten brains of each age (for a total of 60) were rapidly removed, frozen in isopentane at -60°C, then stored at −80°C until sectioned. Coronal, brainstem sections (16 μm thick) were cut at the cryostat (Microm HM550) thaw-mounted on gelatin coated slides (two sections per slide) and stored at -35°C until processed for *in situ* hybridization. Every ninth section was saved for subsequent Nissl staining to verify the position of the SOC.

Riboprobes

GluN1, GluN2A and GluN2B riboprobes were generated in the laboratory. GluN1 primers were designed using Primer 3 online software (Rozen & Skaletsky, 2000) and GluN2A/2B primers were obtained from the Allen Brain Atlas (Lein et al., 2007; see Table 1 for forward and reverse primers used to make each probe). Primer specificity to rat GluN1, GluN2A, and GluN2B mRNAs was confirmed using BLAST (Altschul et al., 1990). Complementary DNA (cDNA) was generated using the polymerase chain reaction (PCR), and this cDNA was inserted into the pGEM T-easy expression vector (Promega, Missisauga, ON, Canada). Sense and antisense probes were transcribed from linearized plasmids

with ∝-35S-UTP (specific activity > 1000 Ci mmol-1; Perkin Elmer, Boston, MA, USA) using appropriate RNA polymerases. The antisense probe produced from the GluN1 cDNA template was 517 base pairs (bp) and complementary to the coding region of rat GluN1 mRNA (bases 2085 – 2602, NM_017010) with 95% identity (Fig 2). The antisense probe produced from the GluN2A cDNA template was 253 bp and complementary to the coding region of rat GluN2A mRNA (bases 652 – 904, NM_012573) with 95% identity (Fig 3). The antisense probe produced from the GluN2B cDNA template was 694 bp and complementary to the coding region of rat GluN2B mRNA (bases 3386 – 4080, NM_012574) with 95% identity (Fig 4). Hybridization with sense probes did not reveal any signal.

Table 1. Forward and reverse primers for GluN1, GluN2A, GluN2B, GluN2C & GluN2D

Probe	Forward	Reverse
GluN1	5'-GTCCTCTGCCATGTGGTTTT-3'	5'-GGACAG-GGACACATTTTGCT-3'
GluN2A	5'-CAGCTG-AAGAAGATCCACTCCT-3'	5'-GCAGTGGTTAAG ATCCCAAGAC-3'
GluN2B	5'-TAGCTA-TAGAGGAGCGCCAATC-3'	5'-CTCGATTTCAT-CAAACTCCCTC-3'
GluN2C	5'-ACGGTACCTAATGGCAGCAC-3'	5'-GCCATGTTGTCAATGTCCAG-3'
GluN2D	5-TTCTTGTCATACATCGAGGTGC-3	5'-CTCCTGGCAGAAGAAGTGGTT-3'

In situ hybridization

Procedures were performed as described by Whitfield et al. (1990) and Foster et al. (2002). Tissue sections were pretreated with 4% formaldehyde for 5 minutes. Sections were then rinsed with phosphate buffer solution (PBS), 0.1 M triethanolamine-HCl (TEA-pH 8.0) and acetylated for 10 minutes with fresh 0.25% acetic acid in triethanolamine (TEA). Tissue sections were dehydrated by rinsing with 70%, 80%, 95%, and 100% ethanol, dilapidated for 5 minutes in chloroform, then rinsed in 100% and 95% ethanol and air dried for approximately 30 minutes. Radiolabeled probes were diluted in hybridization buffer and applied to tissue sections, at approximately 500 000 counts per minute (CPM) per tissue section. Slides were then incubated at 55°C for 16 – 19 hours in a humidified chamber. In order to reduce nonspecific binding of the probe, slides were washed in 20 μg/ml RNase solution (ribonuclease A) for 30 min at room temperature. Slides were then washed in 2x SSC at 50 °C and 0.2x SSC at 55 and 60 °C for 1 h each. Slides were dehydrated using ethanol containing 0.3 M ammonium acetate and air-dried for autoradiography. To ensure that conditions were consistent between sections, all tissue sections for each riboprobe were processed simultaneously.

Autoradiography

Slides and ^{14}C plastic standards containing known amounts of radioactivity were placed in X-ray cassettes and apposed to film for 3 days (GluN1), 11 days (GluN2A) and 5 days (GluN2B). Film was developed in an automatic film

developer (X-OMAT; Eastman Kodak). Digital images were acquired on a Macintosh computer-based image analysis system coupled to a Qiacam digital camera (Quorum Technologies), using a constant illumination light source (Northern Light Precision Illuminator, Imaging Research). Expression of mRNA was quantified with image analysis software from NIH image. In order to unequivocally identify LSO, MNTB and MSO, these structures were first outlined on digital images of adjacent Nissl-stained sections in NIH image. Then, these regions of interest (ROIs) were directly transferred to the *in situ* images (Fig 5). By outlining the structure on the monitor, light transmittance was measured and radioactivity levels (disintegrations per minute [DPM]) were calculated using the Rodbard curve applied to the standards.

Data analysis

The data was analyzed with GraphPad Prism (LaJolla, CA, USA). To determine if mRNA expression levels of GluN1, GluN2A and GluN2B were significantly different between ages, a one-way ANOVA with Tukey's HSD Multiple Comparisons post-hoc tests was used. A mixed model two-way ANOVA with age and nucleus as factors, with repeated measures for nucleus, was also performed to determine if mRNA expression levels were significantly different between nuclei. Statistical significance was set at $p < 0.05$. Data are presented as the mean ± standard error of the mean (SEM).

3. Results

We examined the postnatal developmental mRNA expression of the NMDAR subunits GluN1, GluN2A and GLuN2B in the LSO, MSO and MNTB. We used quantitative *in-situ* hybridization in 10 litters of rats, postnatal day 1 – 36 (P1, 8, 15, 22, 29 and 36). Representative *in situ* images of GluN1, GluN2A and GluN2B mRNA expression during postnatal development in auditory brainstem are shown in Figure 6.

Postnatal developmental expression of GluN1 mRNA

In all three nuclei, GluN1 mRNA expression was regulated similarly. In the LSO, GluN1 mRNA expression was relatively stable from P1 to P15, then declined by approximately 35% between P22 and P36 (Table 2 in Appendix A, Fig 7) (one-way ANOVA, $F_{(5, 54)} = 3.69$, $p = 0.0061$). Post-hoc tests indicated that GluN1 mRNA expression levels at P1 (M = 898.13 ± 167.04) were significantly higher than expression levels at P36 (M = 373.60 ± 64.17). GluN1 levels were thus significantly higher at birth when compared to P36 ($p < 0.05$). In the MNTB, GluN1 expression increased slightly from P1 to P15, then declined to P1 levels at P22 and remained relatively stable thereafter (Table 1, Fig 8) (one-way ANOVA, $F_{(5,54)} = 3.04$, $p = 0.0172$). A post-hoc comparison revealed that GluN1 mRNA expression levels in the MNTB were significantly higher at P15 (M = 1548.88 ± 190.45) than levels at P36 (805.93 ± 102.00). In the MSO, GluN1 expression

levels remained relatively stable between P1 and P15, then declined by about 50% between P15 and P36 (Table 1, Fig 9) (one-way ANOVA, $F_{(5,54)} = 5.01$, $p = 0.0008$) and GluN1 expression was significantly higher at P1 (M = 967.94 ± 129.44) than at P36 (M = 432.40 ± 69.12) and levels at P8 (M = 1116.94 ± 133.51) were significantly higher than levels at P29 (M = 539.13 ± 148.98) and P36. GluN1 expression levels at P15 (M = 984.12 ± 131.13) were also significantly higher than levels at P36. Thus, GluN1 mRNA expression levels in the MSO were significantly higher during the first three postnatal weeks of development. A two-way ANOVA showed that there were main effects of age ($F_{(5, 108)} = 3.70$, $p = 0.0006$) and nucleus ($F_{(2, 108)} = 148.87$, $p < 0.0001$) with an interaction between both factors ($F_{(10, 108)} = 3.65$, $p = 0.0003$). Although there were individual differences in GluN1 expression patterns during the ages examined, all three nuclei exhibited the same general trend. GluN1 expression decreased during the first five postnatal weeks. Because the GLuN1 is an obligatory subunit of the NMDAR (Cull-Candy et al., 2001; Ishii et al., 1993), GluN1 mRNA expression can be used as an indicator of overall NMDAR expression. Thus, in all three nuclei, NMDAR expression levels decreased during the first five postnatal weeks of auditory development.

Postnatal developmental expression of GluN2B mRNA

In the LSO, GluN2B expression levels were highest at P1, and declined by about 75% between P1 and P36 (Table 3 in Appendix A, Fig 10) (one-way

ANOVA, $F_{(5,54)} = 39.62$, $p < 0.0001$). Using Tukey's HSD post-hoc tests, we found that GluN2B mRNA expression levels were highest at P1 (M = 1021.49 ± 104.67) when compared to levels at P8 (M = 717.24 ± 60.86), P15 (M = 367.68 ± 14.21), P22 (M = 269.91 ± 9.11), P29 (254.50 ± 16.46), and P36 (254.27 ± 13.07). GluN2B expression levels were also significantly higher at P8 when compared to all older ages. Thus, in the LSO, GluN2B levels were highest during the first postnatal week of development. In the MNTB, GluN2B expression decreased by about 30% from P1 to P8, and declined to low levels between P8 and P36 (Table 3, Fig 11) (one-way ANOVA, $F_{(5,54)} = 44.19$, $p < 0.0001$). Tukey's post-hoc tests indicated that GluN2B mRNA expression levels were highest at P1 (M = 1069.17 ± 100.95) when compared to expression levels at all other ages. GluN2B levels at P8 (M = 721.93 ± 57.11) were also significantly higher than levels at P15 (M = 383.42 ± 25.14), P22 (M = 270.79 ± 17.73), P29 (M = 244.48 ± 19.45), and P36 (M = 277.43 ± 16.28). In the MNTB, similar to what had been seen in the LSO, GluN2B mRNA levels were highest during the first postnatal week. In the MSO, GluN2B expression was highest from P1 to P8, then expression levels dropped by approximately 50% at P15, remaining stable to P36 (Table 3, Fig 12) (one-way ANOVA, $F_{(5,54)} = 42.05$, $p < 0.0001$). Post-hoc tests showed that GluN2B mRNA expression levels at P1 (M = 844.19 ± 66.66) and P8 (M = 834.09 ± 78.65) were significantly higher than levels at P15 (M = 332.37 ± 21.78), P22 (M = 271.24 ± 10.10), P29 (M = 280.00 ± 20.10), and P36 (M = 259.79 ± 11.39). A two-way ANOVA showed a main effect of age ($F_{(5, 108)} = 57.84$, $p < 0.0001$) but not

nucleus ($F_{(2, 108)}$ = 0.86, p = 0.4259), with an interaction between both factors ($F_{(10, 108)}$ = 3.63, p = 0.0003). Thus, all three nuclei exhibited similar patterns of GluN2B expression through development: GluN2B mRNA expression was highest during the first postnatal week, and declined during the first five postnatal weeks.

Postnatal developmental expression of GluN2A mRNA

In the LSO, GluN2A expression increased by approximately 100% between P1 and P15, after which GluN2A levels declined by about 33% at P22 and remained stable to P36 (Table 4 in Appendix A, Fig 13) (one-way ANOVA, $F_{(5,54)}$ = 5.65, p = 0.0003). Tukey's HSD post-hoc tests revealed that GluN2A expression levels were significantly higher at P15 (M = 204.08 ± 24.06) than levels at P1 (M = 102.79 ± 9.47), P8 (M = 133.96 ± 15.69), P22 (M = 135.97 ± 7.83), and P36 (M = 138.71 ± 7.52). Thus, the amount of GluN2A mRNA in the LSO increased between birth and the second postnatal week, and then declined to moderate levels. In the MNTB, GluN2A expression remained relatively stable at high levels between P1 and P8, then declined by approximately 50% by P15, remaining stable thereafter (Table 2, Fig 14) (one-way ANOVA, $F_{(5,54)}$ = 18.07, p < 0.0001). Post-hoc analyses revealed that GluN2A mRNA expression levels at P1 (M = 322. 09 ± 32.15) and P8 (M = 396.66 ± 18.94) were significantly higher than levels at P15 (M = 209.52 ± 22.76), P22 (M = 157.91 ± 13.55), P29 (M = 185.18 ± 20.84) and P36 (M = 200.18 ± 18.78). Thus, GluN2A mRNA expression

was highest during the first week of development in the MNTB. In the MSO, GluN2A expression increased by approximately 100% between P1 and P8, and expression levels remained stable thereafter (Table 2, Fig 15) (one-way ANOVA, $F_{(5,54)} = 8.43$, $p < 0.0001$). Tukey's HSD post-hoc tests revealed that GluN2A mRNA expression levels at P1 (M = 102.25 ± 10.33) were significantly lower than levels at P8 (M = 202.75 ± 23.08), P15 (M = 206.62 ± 10.20), P22 (M = 177.45 ± 8.58), P29 (M = 197.36 ± 12.20) and P36 (M = 196.96 ± 12.42). A two-way ANOVA indicated that there were main effects of age ($F_{(5, 108)} = 6.54$, $p < 0.0001$) and nucleus ($F_{(2, 108)} = 76.39$, $p < 0.0001$) with an interaction between the two ($F_{(10, 108)} = 20.26$, $p < 0.0001$). In the LSO, GluN2A levels increased during the first two postnatal weeks, then decreased to moderate levels. In the MNTB, GluN2A levels were highest during the first postnatal week, and then declined to remain stable at moderate levels. In the MSO, a distinct expression pattern was seen; GluN2A mRNA levels were lowest at birth and then increased to moderate levels by the end of first postnatal week.

Expression of GluN2A & GluN2B mRNA between nuclei

In both the LSO and MSO, the ratio of GluN2A to GluN2B increased approximately 3-fold between P8 and P15 (Fig 16). In the MNTB, a 2-fold increase in the GluN2A:GluN2B ratio occurred a week earlier, between P1 and P8 (Fig 16). This is consistent with a developmental switch from GluN2B-

containing NMDARs to GluN2A-containing NMDARs. This switch appears to occur a week earlier in the MNTB when compared to the LSO or MSO.

To compare relative expression patterns of GluN1, GluN2A and GluN2B between nuclei, we normalized the average DPM values for GluN1, GluN2A and GluN2B throughout postnatal development in the MNTB and LSO to the average DPM values for the ipsilateral MSO in the same tissue section. In addition, for all three subunits, we normalized the average DPM values of the MNTB to the average DPM values of the LSO in the same section. GluN1 values in the MNTB and LSO normalized to the MSO exhibited similar expression patterns throughout postnatal development (Fig 17). However, relative values of GluN1 during the first five postnatal weeks were generally higher in the MNTB than in the LSO. GluN1 values in the MNTB normalized to LSO increased slightly from P8 to adulthood (Fig 18). GluN2B values in the MNTB and LSO normalized to MSO exhibited a similar expression pattern throughout postnatal development (Fig 19). GluN2B values in the MNTB normalized to the LSO also exhibited the same general trend as seen with GluN1 values in the MNTB and LSO normalized to the MSO (Fig 20). The GluN2A subunit exhibited a completely distinct expression pattern throughout postnatal development in the MNTB when compared to the LSO and MSO. Normalizing the DPM values of GluN2A in the MNTB and LSO to the MSO made postnatal developmental differences more apparent. In the MNTB, GluN2A values normalized to MSO were highest at P1, and then decreased between P1 and P15 (Fig 21). GluN2A values in the LSO normalized to MSO did not show the

same difference in expression patterns. GluN1 mRNA expression was therefore higher in the MNTB than in the LSO and MSO during the first two postnatal weeks. GluN2A values in the MNTB normalized to the LSO exhibited a similar expression pattern to GluN2A values normalized to the MSO (Fig 22). GluN2A values were highest during the first two postnatal weeks. Notably, GluN2A mRNA expression in the MNTB normalized to the LSO decreased between P8 and P15, whereas expression normalized to the MSO decreased between P1 and P15.

Other Studies

When beginning this study, we had hoped to also examine postnatal developmental expression of GluN2C and GluN2D in the LSO, MSO and MNTB. The GluN2C and -2D probes proved difficult to prepare (troubleshooting issues are outlined in the discussion).

4. Figures

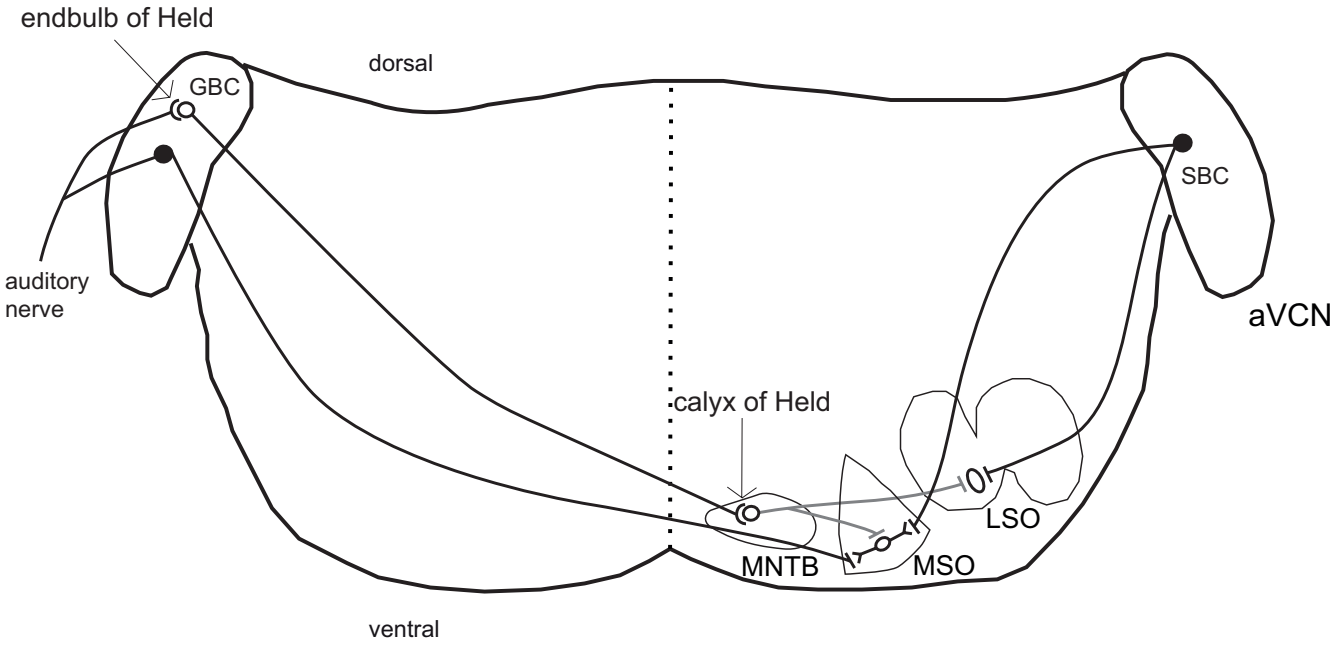

Figure 1: Schematic of coronal brainstem slice, showing major inputs to the mammalian LSO, MSO and MNTB. Globular bushy cells (GBC) and spherical bushy cells (SBC) receive excitatory (black line) inputs from the auditory nerve, forming the endbulb of Held synapse on GBC and SBC neurons. The GBCs send excitatory inputs to the contralateral MNTB, forming the one-to-one calyx of Held synapse onto each MNTB principal cell. The SBCs send excitatory inputs to the ipsilateral LSO, as well as the ipsilateral and contralateral MSO. The MNTB sends inhibitory inputs (gray line) to the MSO and LSO. In the mature system, the MSO computes ITDs by integrating the excitatory inputs from both SBCs, as well as the inhibitory (mainly glycinergic) input from the MNTB. It is important to note that the MSO also receives an inhibitory input from a smaller structure, the LNTB (not shown in this schematic). Neurons in the MSO have a bipolar morphology, with the soma in the center (as depicted). The ipsilateral excitatory input to the MSO synapses on lateral dendrites, whereas the contralateral excitatory inputs synapse onto medial dendrites. The inhibitory inputs to the MSO synapse onto the soma. The LSO computes ILDs by integrating the excitatory and inhibitory inputs to LSO principal cells. The mature LSO is tonotopically organized such that each LSO principal cell is excited and inhibited by the same sound frequency. For simplicity, only one principal cell is shown in each structure.

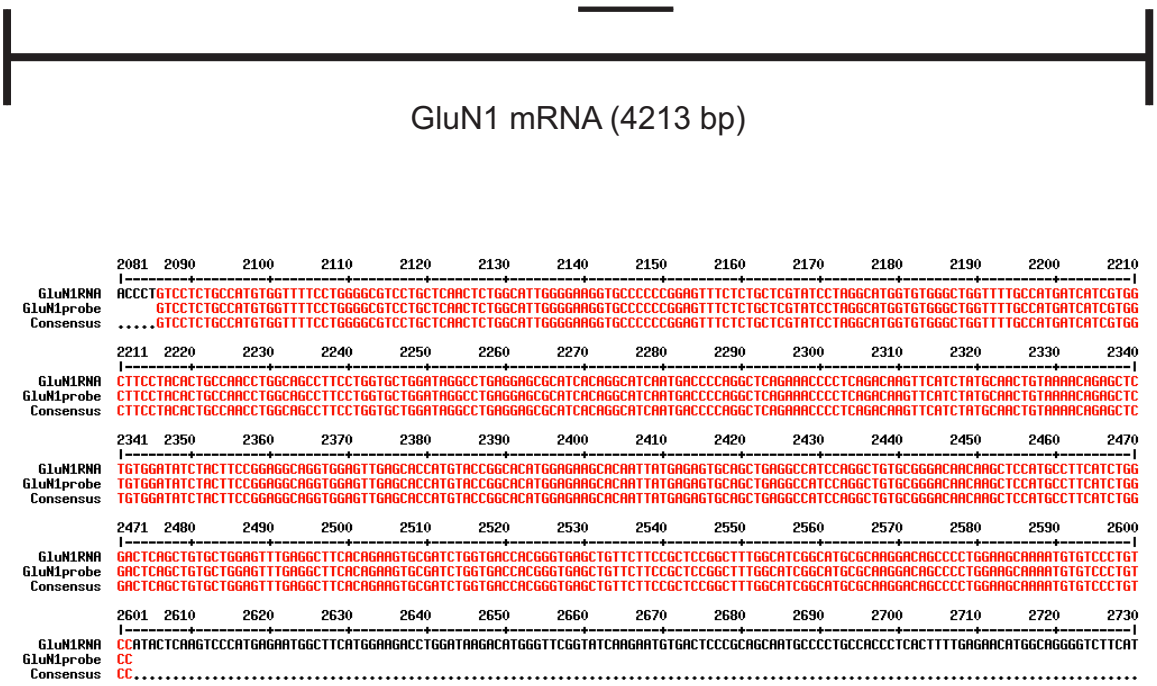

Figure 2: GluN1 riboprobe sequence matched to GluN1 mRNA. Top panel with the line depicts the GluN1 riboprobe (517 bp) that was designed to be complementary to GluN1 mRNA. Bottom panel depicts, in red, the base pairs that are complementary to GluN1 mRNA. It can be seen that the GluN1 riboprobe is complementary to base pairs 2085 – 2602 in GluN1 mRNA with 95% identity.

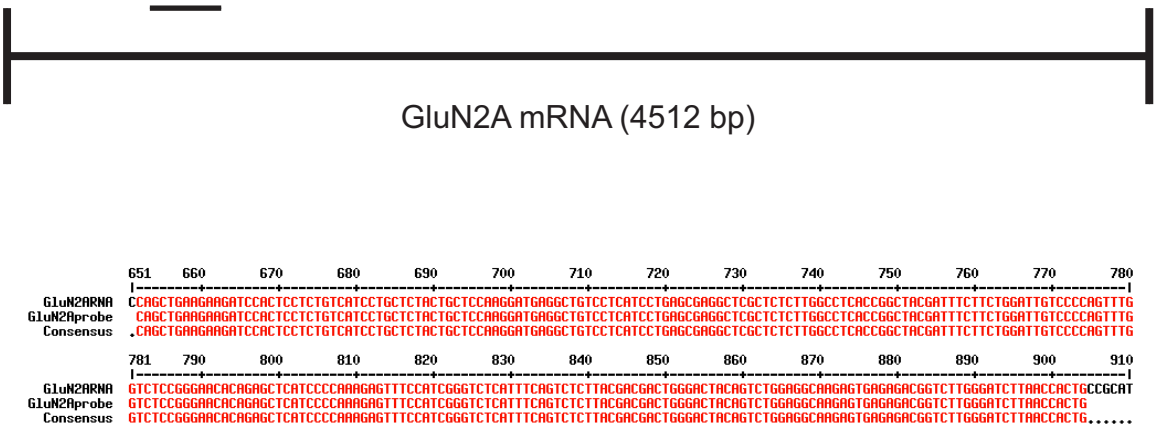

Figure 3: GluN2A riboprobe sequence matched to GluN2A mRNA. Top panel with the line depicts the GluN2A riboprobe (253 bp) that was designed to be complementary to GluN2A mRNA. Bottom panel depicts, in red, the base pairs that are complementary to GluN2A mRNA. It can be seen that the GluN2A riboprobe is complementary to base pairs 652 - 904 in GluN2A mRNA with a 95% identity.

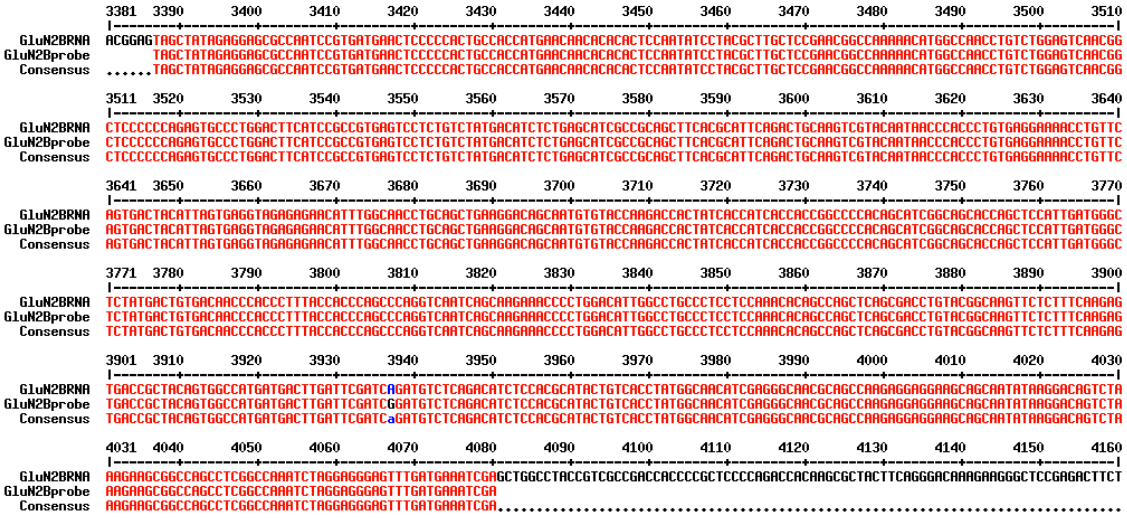

Figure 4: GluN2B riboprobe sequence matched to GluN2B mRNA. Top panel with the line depicts the GluN2B riboprobe (694 bp) that was designed to be complementary to GluN2B mRNA. Bottom panel depicts, in red, the base pairs that are complementary to GluN2B mRNA. The base pairs in blue show non-matched base pairs. It can be seen that the GluN2B riboprobe is complementary to base pairs 3386 – 4080 in GluN2B mRNA with a 95% identity.

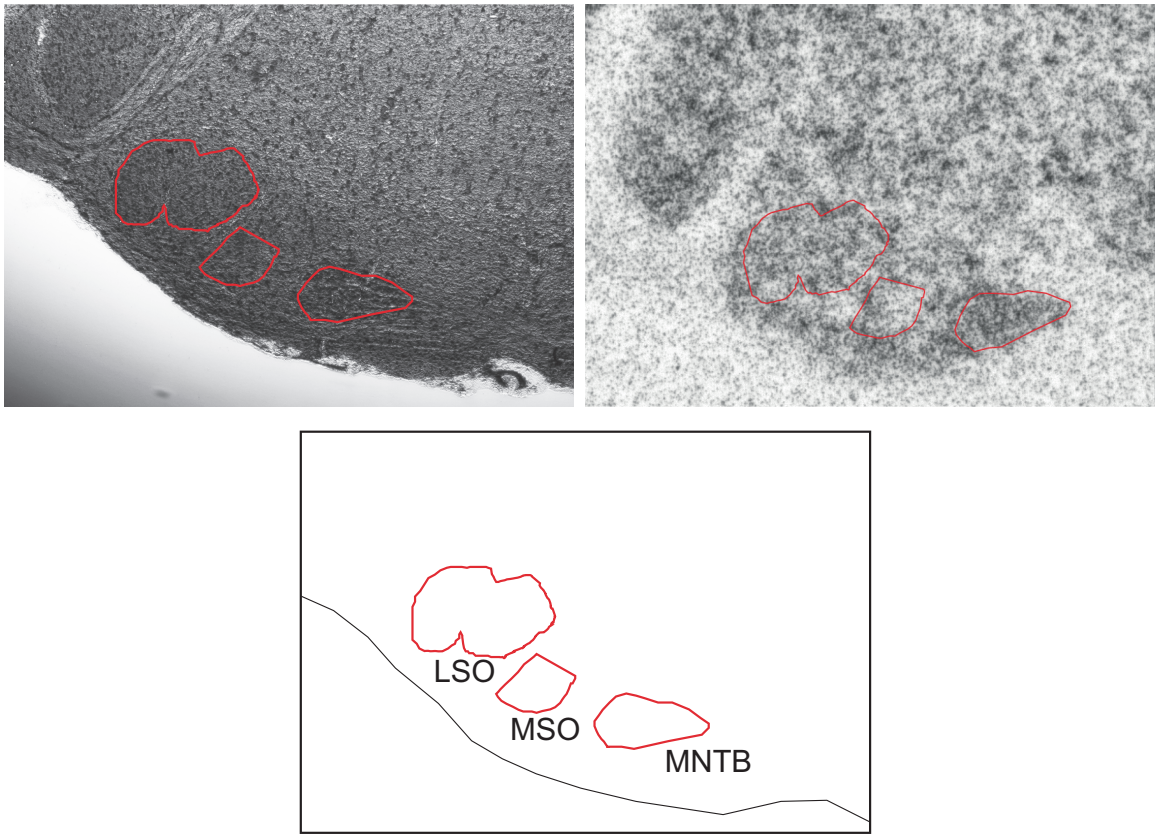

Figure 5: Nissl-stained section and adjacent *in-situ* image showing outlines of LSO, MSO and MNTB. Nissl-stained section (on the left, P15 tissue) and *in-situ* image from adjacent tissue section. On the Nissl-stained section, the three nuclei were identified and an outline was drawn on NIH image. These outlines, or regions of interest (ROIs), were transferred to the adjacent *in-situ* image. NIH image was then used to calculate DPM values. Bottom image identifies the outlines that correspond to the specific nuclei.

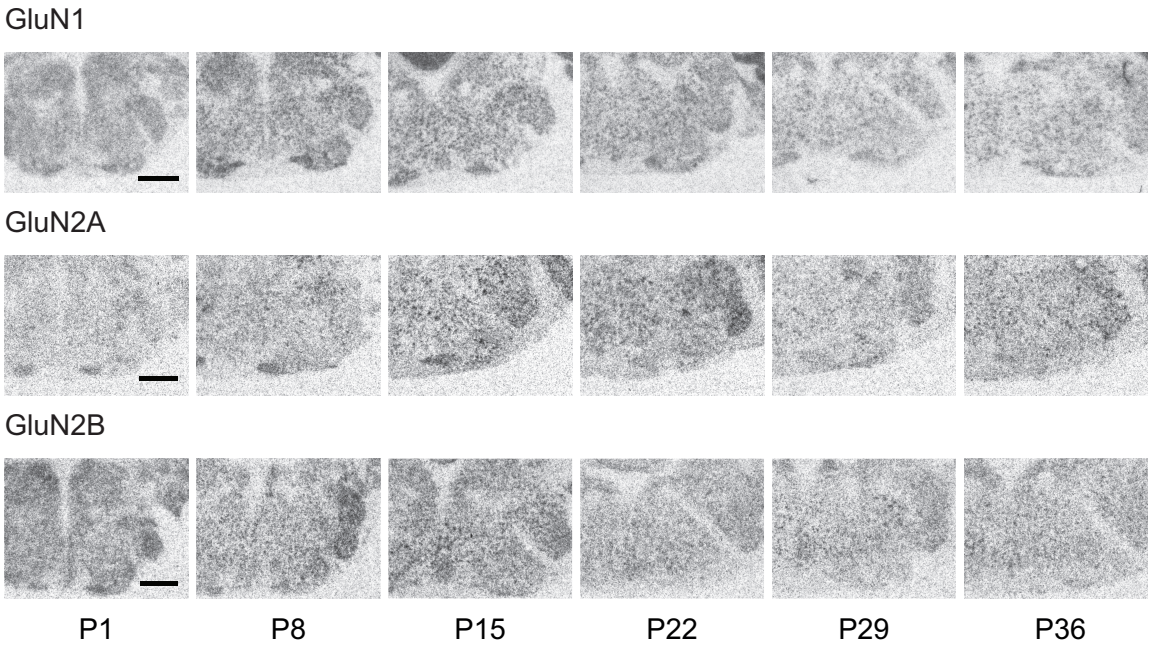

Figure 6: Representative *in situ* images of GluN1, GluN2A and GluN2B mRNA expression during postnatal development in auditory brainstem. Scale bar = 1 mm.

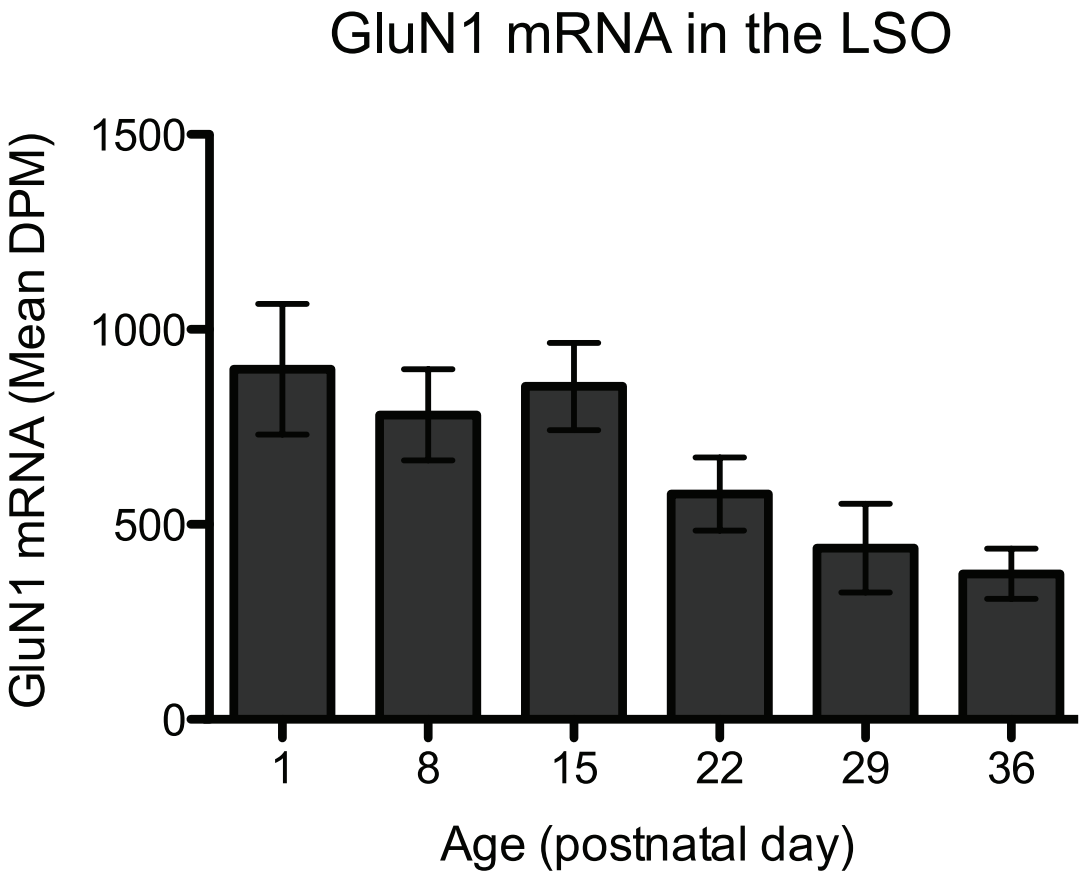

Figure 7: Postnatal developmental expression of GluN1 mRNA in the LSO. GluN1 mRNA expression levels remain relatively stable between P1 and P15, then decline to P36 (one-way ANOVA, $F_{(5, 54)} = 3.69$, $p = 0.0061$). GluN1 mRNA expression at P1 is significantly higher than expression at P36 (Tukeys HSD post-hoc test, $p < 0.05$). Values are means ± SEM.

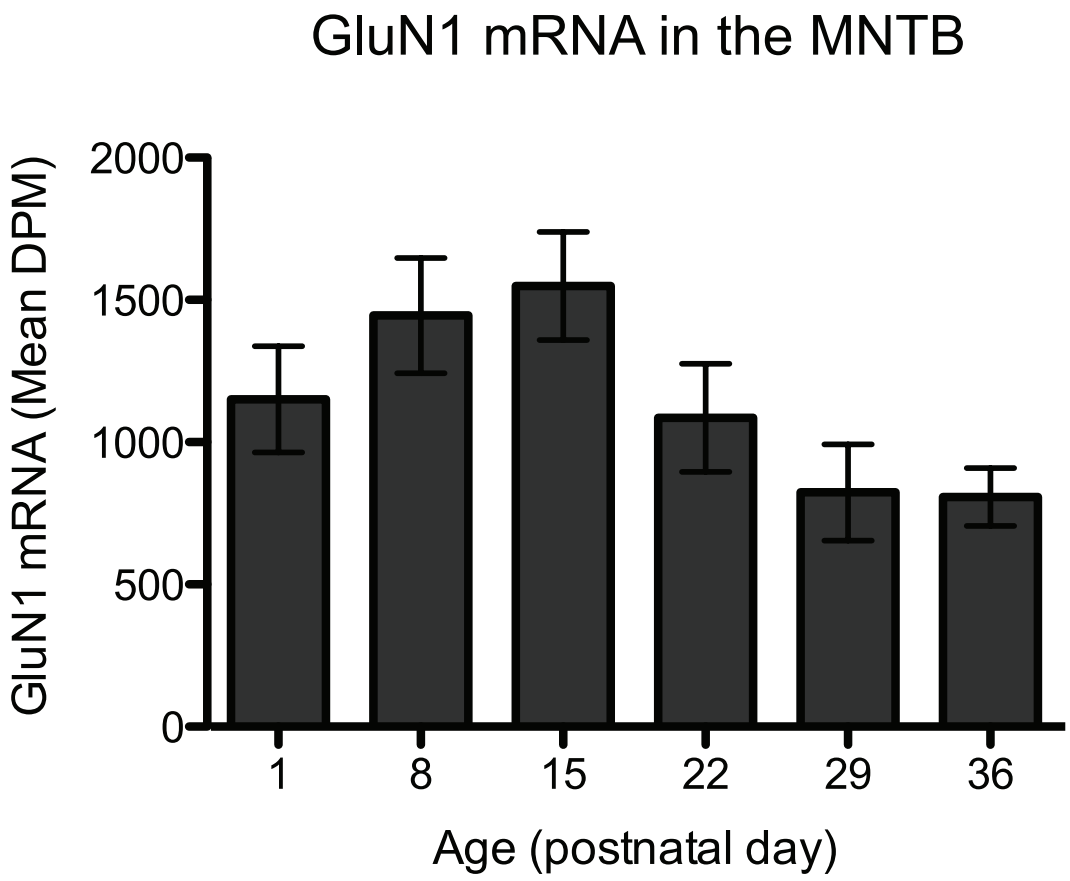

Figure 8: Postnatal developmental expression of GluN1 mRNA in the MNTB. GluN1 mRNA levels increase slightly between P1 and P15, then decline to P1 values at P22, remaining stable thereafter (one-way ANOVA, $F_{(5,54)} = 3.04$, $p = 0.0172$). GluN1 mRNA levels are highest at P15, then decline to P36 (Tukeys post-hoc test, $p < 0.05$). Values are means ± SEM.

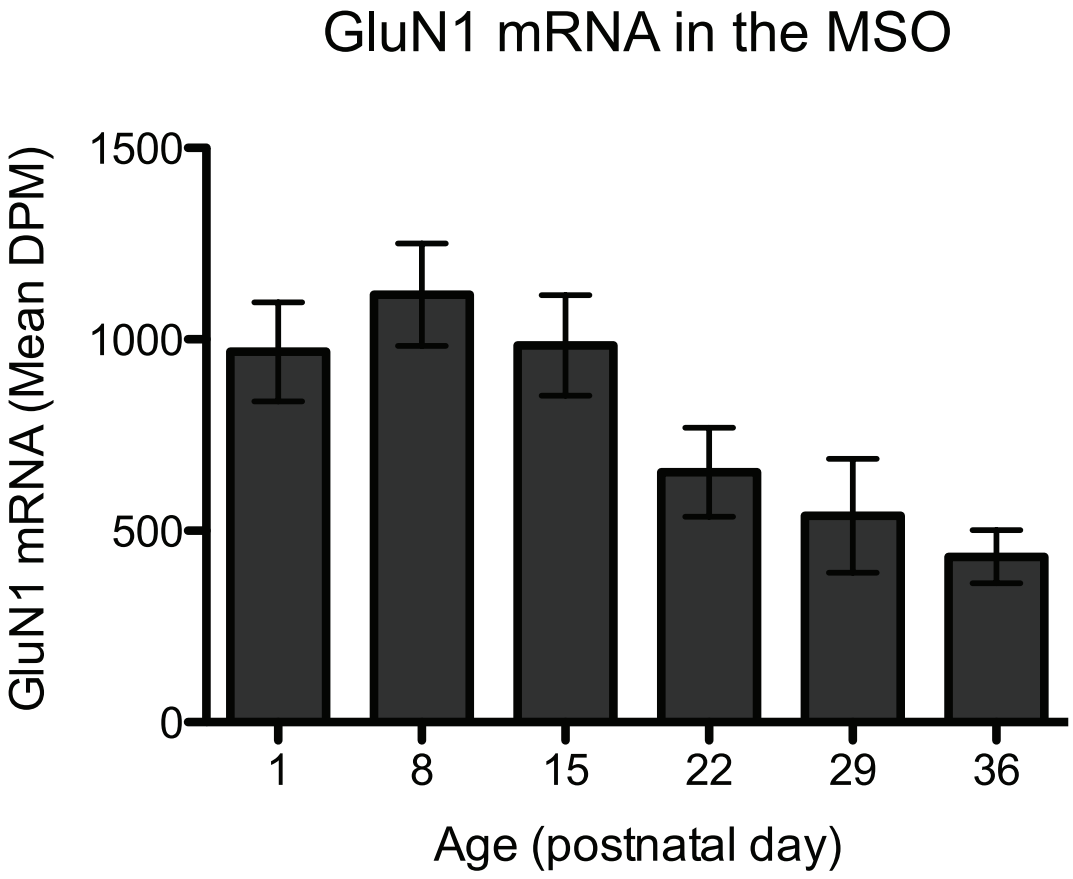

Figure 9: Postnatal developmental expression of GluN1 mRNA in the MSO. GluN1 expression levels remain relatively stable between P1 and P15, then decline by about 50% from P15 to P36 (one-way ANOVA, $F_{(5,54)} = 5.01$, $p = 0.0008$). GluN1 mRNA expression is significantly higher at P1, P8 and P15 when compared to P36 (Tukey's post-hoc test, $p < 0.05$). GluN1 mRNA levels at P8 are also significantly higher than levels at P29 (Tukey's post-hoc test, $p < 0.05$). Values are means ± SEM.

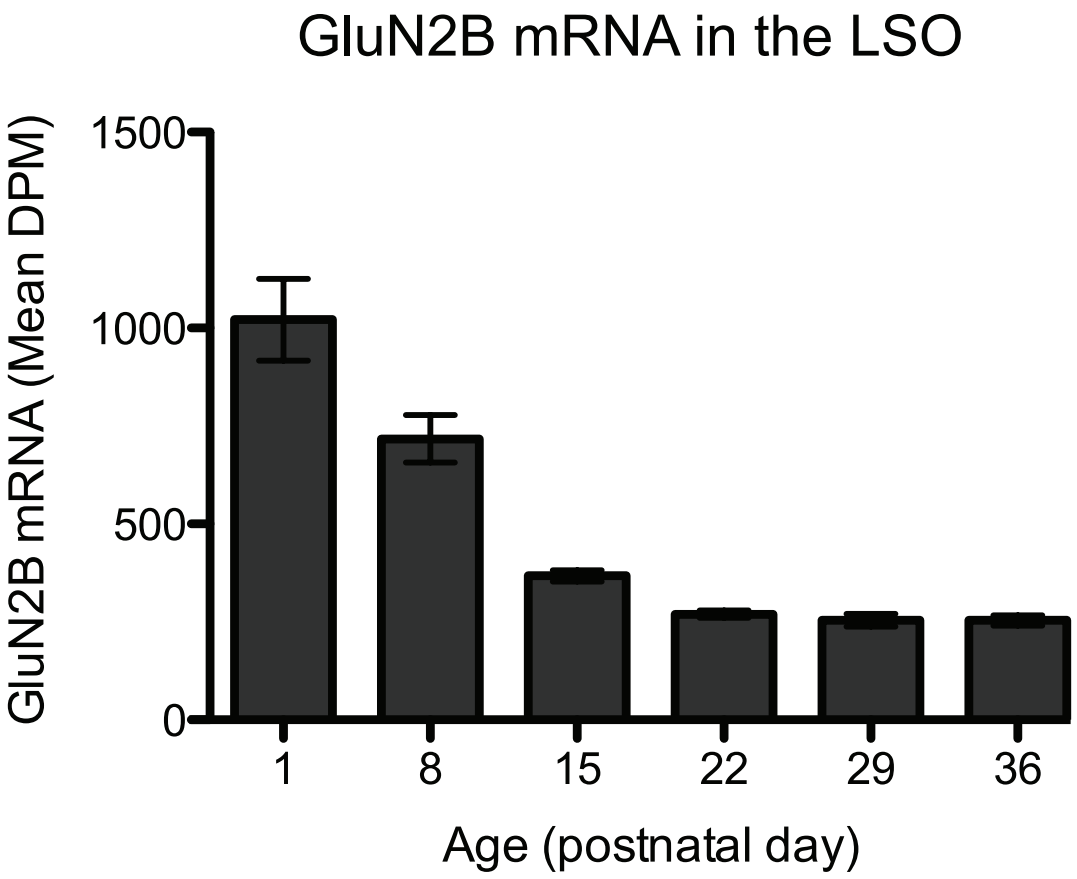

Figure 10: Postnatal developmental expression of GluN2B mRNA in the LSO. GluN2B expression levels decline by about 75% between P1 and P36 (one-way ANOVA, $F_{(5,54)} = 39.62$, $p < 0.0001$). GluN2B mRNA levels are significantly highest at P1 and levels at P8 are significantly higher than levels at all older ages (Tukey's post-hoc tests, $p > 0.05$). Values are means ± SEM.

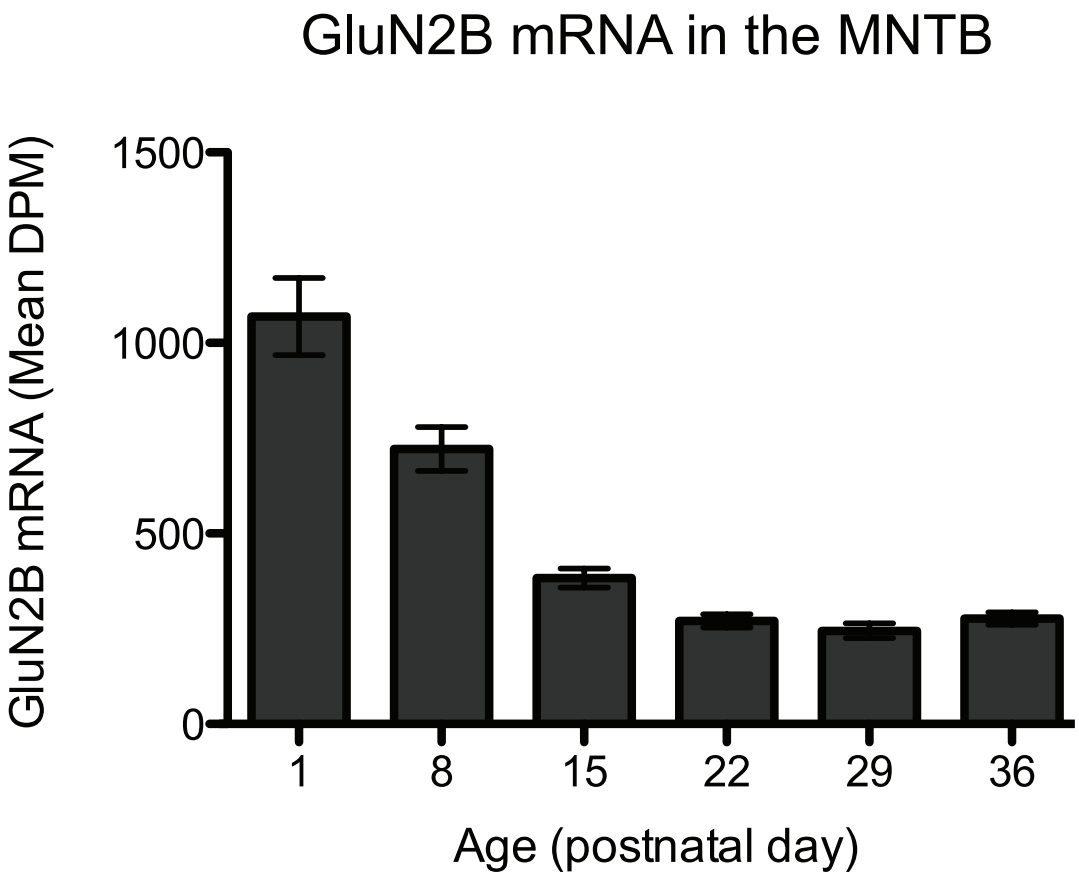

Figure 11: Postnatal developmental expression of GluN2B mRNA in the MNTB. GluN2B mRNA levels are highest at P1, then decline by about 50% and levels remain relatively stable to P36 (one-way ANOVA, $F_{(5,54)} = 44.19$, $p < 0.0001$). GluN2B mRNA levels are significantly highest at P1, and mRNA levels P8 are also significantly higher than levels at all older ages (Tukeys post-hoc test, $p > 0.05$). Values are means ± SEM.

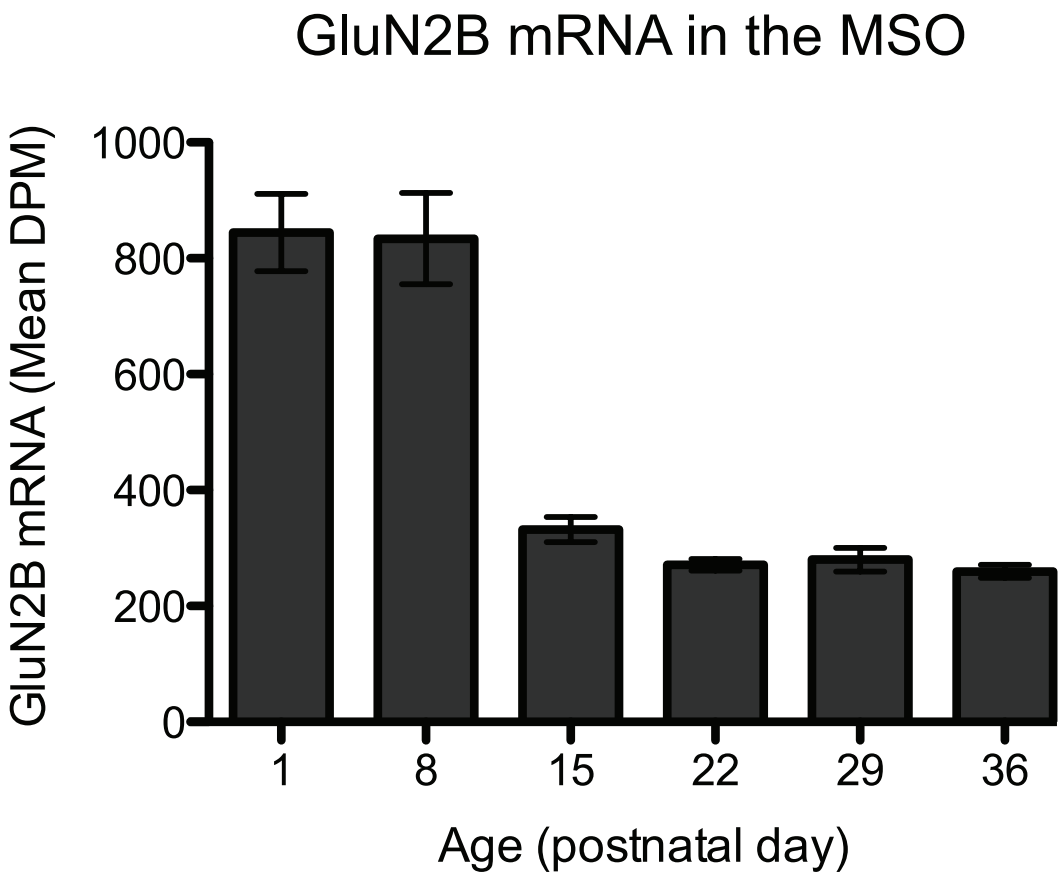

Figure 12: Postnatal developmental expression of GluN2B mRNA in the MSO. GluN2B expression levels are highest between P1 and P8, then levels decline by about 50% by P15 remaining relatively stable to P36 (one-way ANOVA, $F_{(5,54)}$ = 42.05, $p < 0.0001$). GluN2B mRNA expression is significantly higher at P1 and P8 when compared to levels between P15 to P36 (Tukey's post-hoc test, $p < 0.05$). Values are means ± SEM.

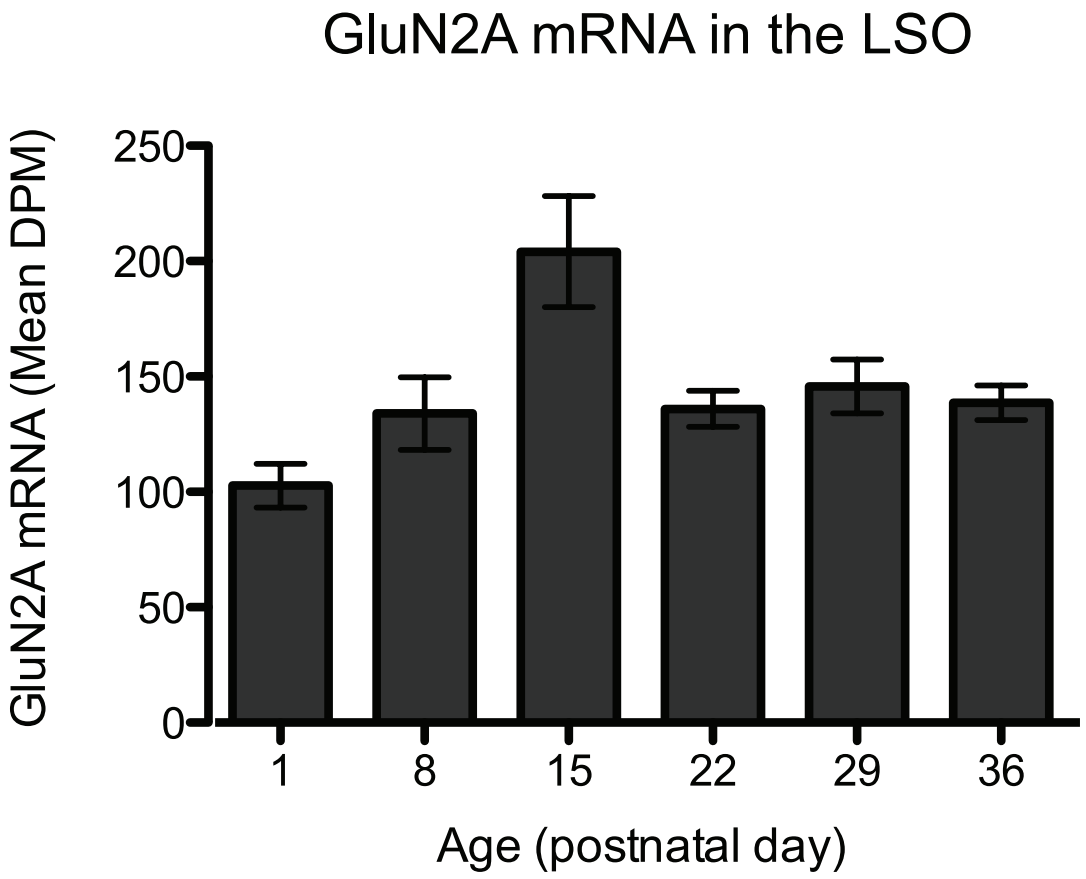

Figure 13: Postnatal developmental expression of GluN2A mRNA in the LSO. GluN2A mRNA levels increase by approximately 100% between P1 and P15, then decline by about 33% by P22, remaining stable thereafter (one-way ANOVA, $F_{(5,54)} = 5.65$, $p = 0.0003$). GluN1 mRNA expression is significantly higher at P15 than at P1, P8, P22 and P36 (Tukey's post-hoc test, $p < 0.05$). Values are means ± SEM.

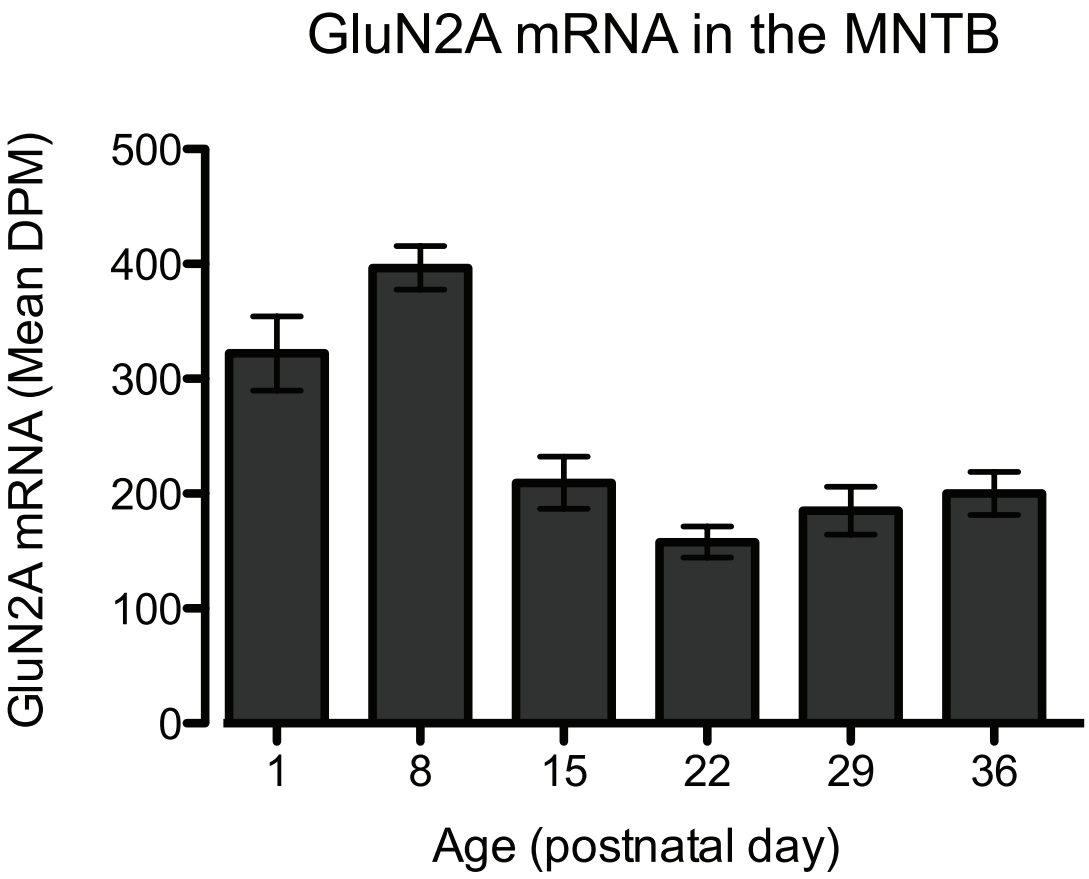

Figure 14: Postnatal developmental expression of GluN2A mRNA in the MNTB. GluN2A mRNA levels remain relatively stable between P1 and P8, then decline by about 50% between P8 and P15. After P15, GluN2A levels remain relatively stable (one-way ANOVA, $F_{(5,54)} = 18.07$, $p < 0.0001$). GluN2A mRNA levels are significantly higher at P1 and P8 than mRNA levels at all older ages (Tukey's post-hoc test, $p > 0.05$). Values are means ± SEM.

Figure 15: Postnatal developmental expression of GluN2A mRNA in the MSO. GluN2A expression levels increase by approximately 100% between P1 and P8, then levels remain relatively stable to P36 (one-way ANOVA, $F_{(5,54)} = 8.43$, $p < 0.0001$). GluN2A mRNA levels are significantly lower at P1 when compared to all older ages (Tukeys post-hoc test, $p > 0.05$). Values are means ± SEM.

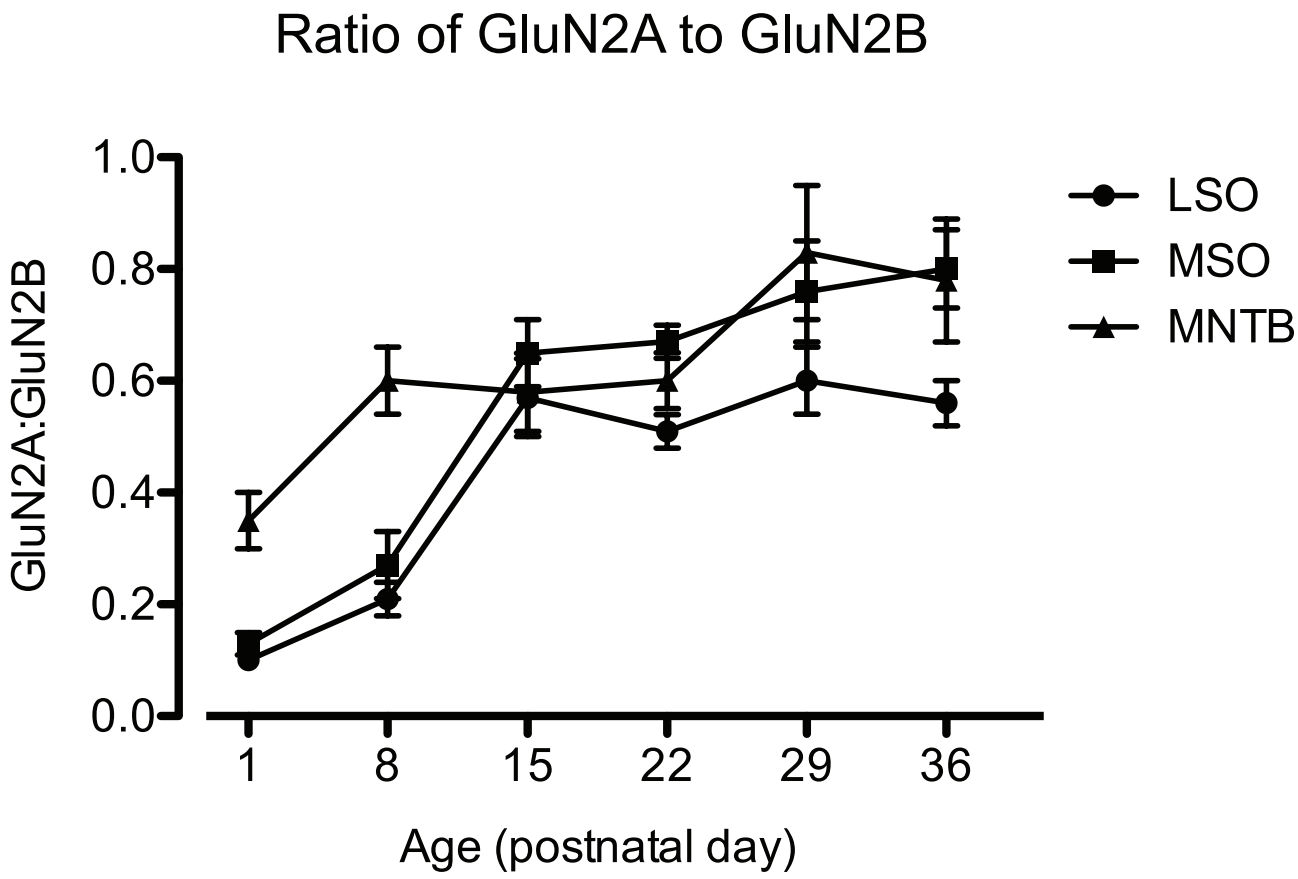

Figure 16: Ratio of GluN2A to GluN2B during postnatal development in the LSO, MSO and MNTB. A 3-fold increase in ratio of GluN2A to GluN2B occurs between P8 and P15 in both the LSO and MSO. A similar 3-fold increase in the ratio is seen in the MNTB, but occurs a week earlier, between P1 and P8. Ratio of GluN2A to GluN2B shown ± SEM.

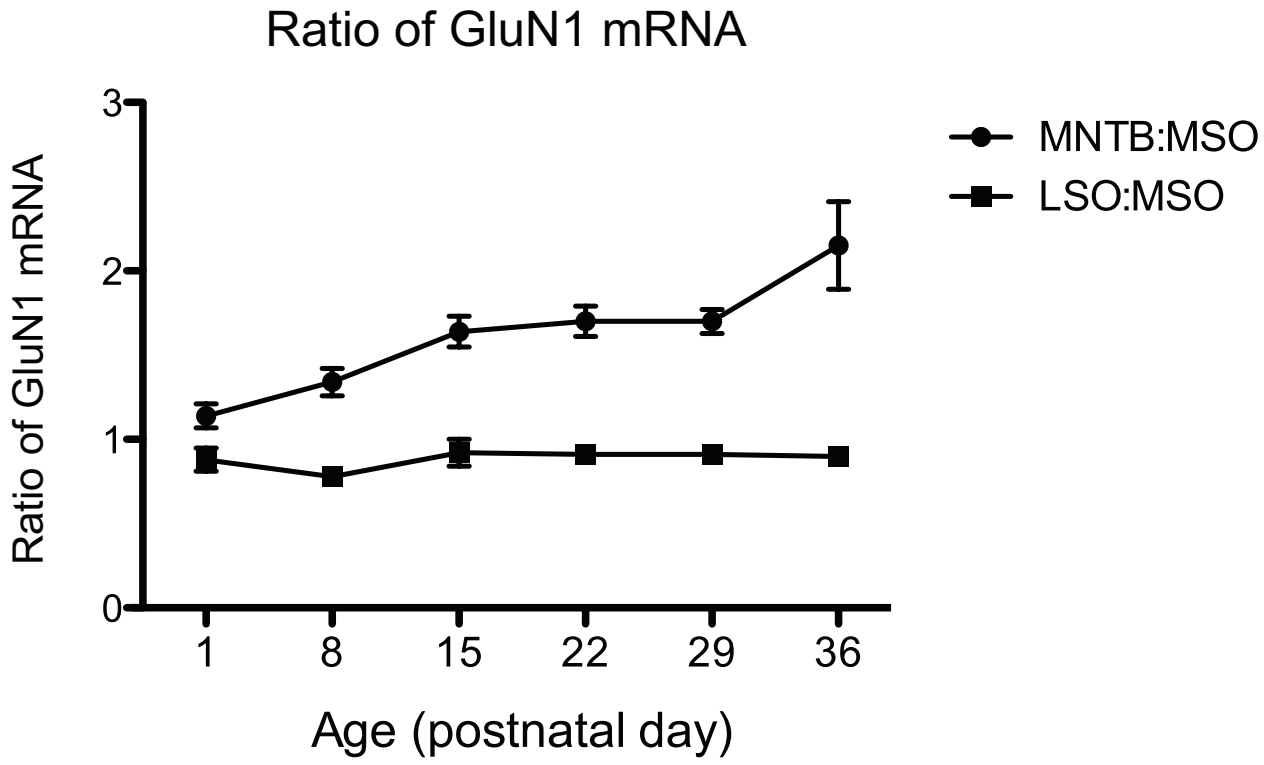

Figure 17: GluN1 mRNA expression in the MNTB and LSO normalized to GluN1 expression in the MSO. GluN1 expression is relatively higher in the MNTB than in the LSO. GluN1 expression patterns are similar in both MNTB and LSO throughout postnatal development.

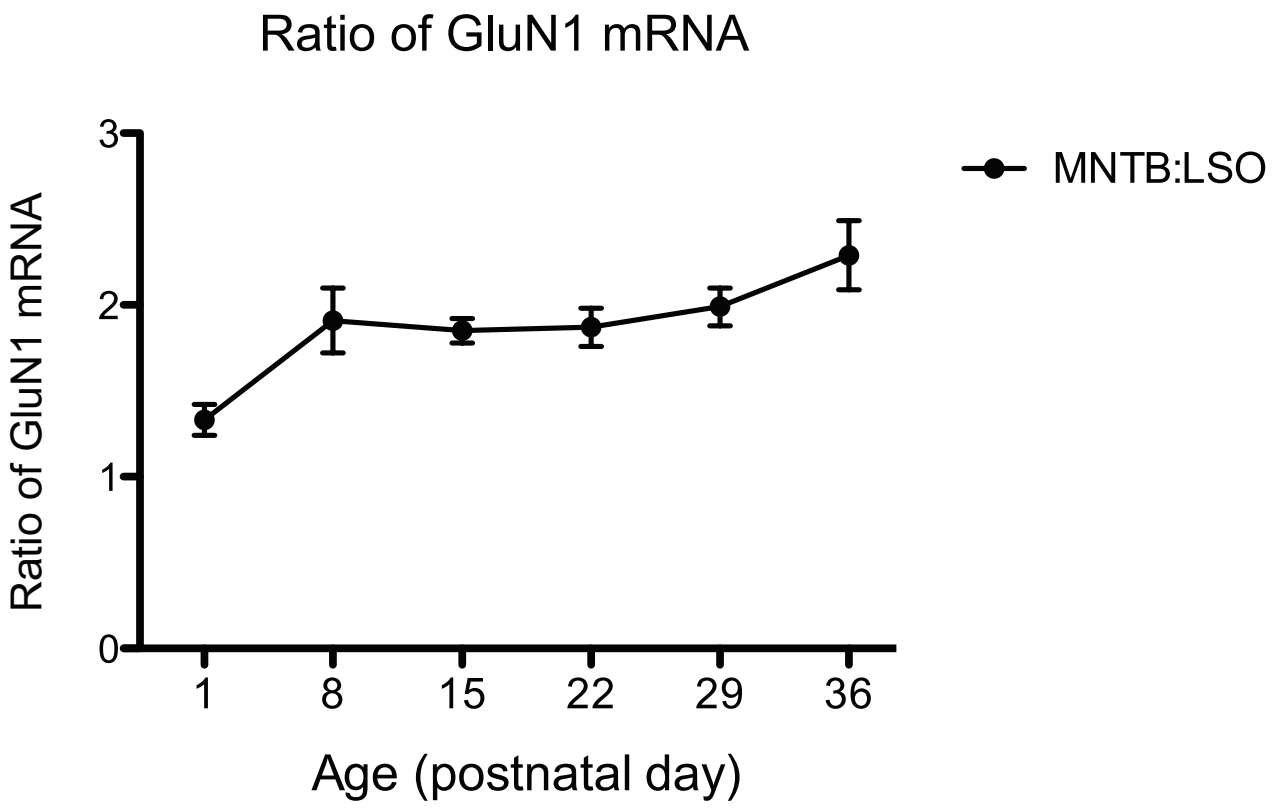

Figure 18: GluN1 mRNA expression in the MNTB normalized to GluN1 expression in the LSO. GluN1 expression increased slightly after P8, but overall trend throughout postnatal development is similar to GluN1 expression in MNTB normalized to MSO.

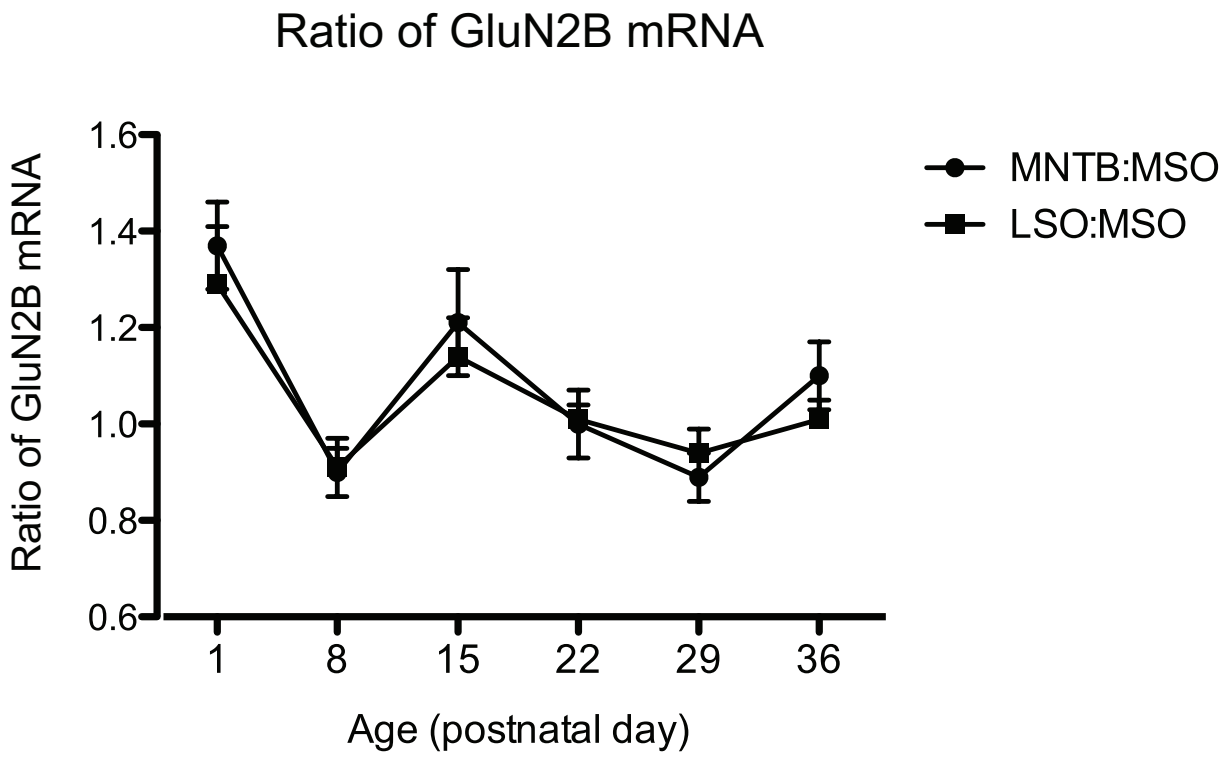

Figure 19: GluN2B mRNA expression in the MNTB and LSO normalized to GluN2B expression in the MSO. Both MNTB and LSO exhibit a similar trend throughout postnatal development.

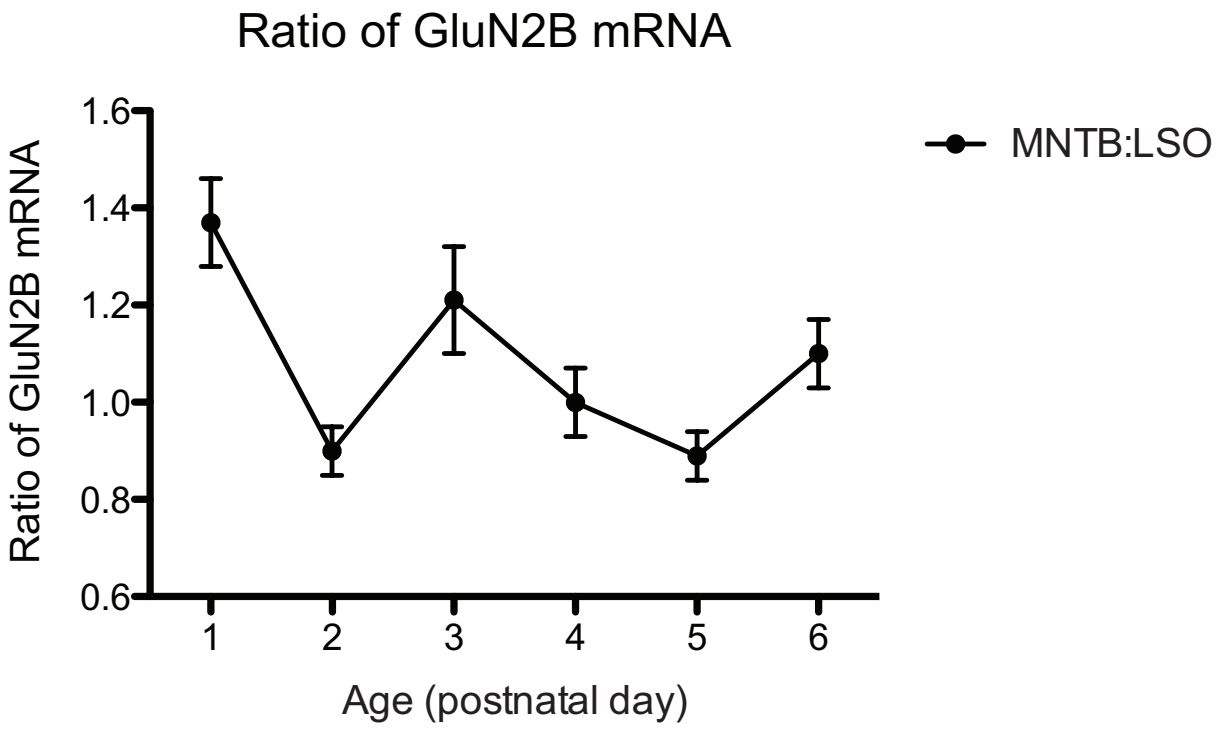

Figure 20: GluN2B mRNA expression in the MNTB normalized to GluN2B expression in the LSO. GluN2B expression exhibits the same pattern throughout postnatal development as seen with GluN2B expression in the MNTB normalized to MSO.

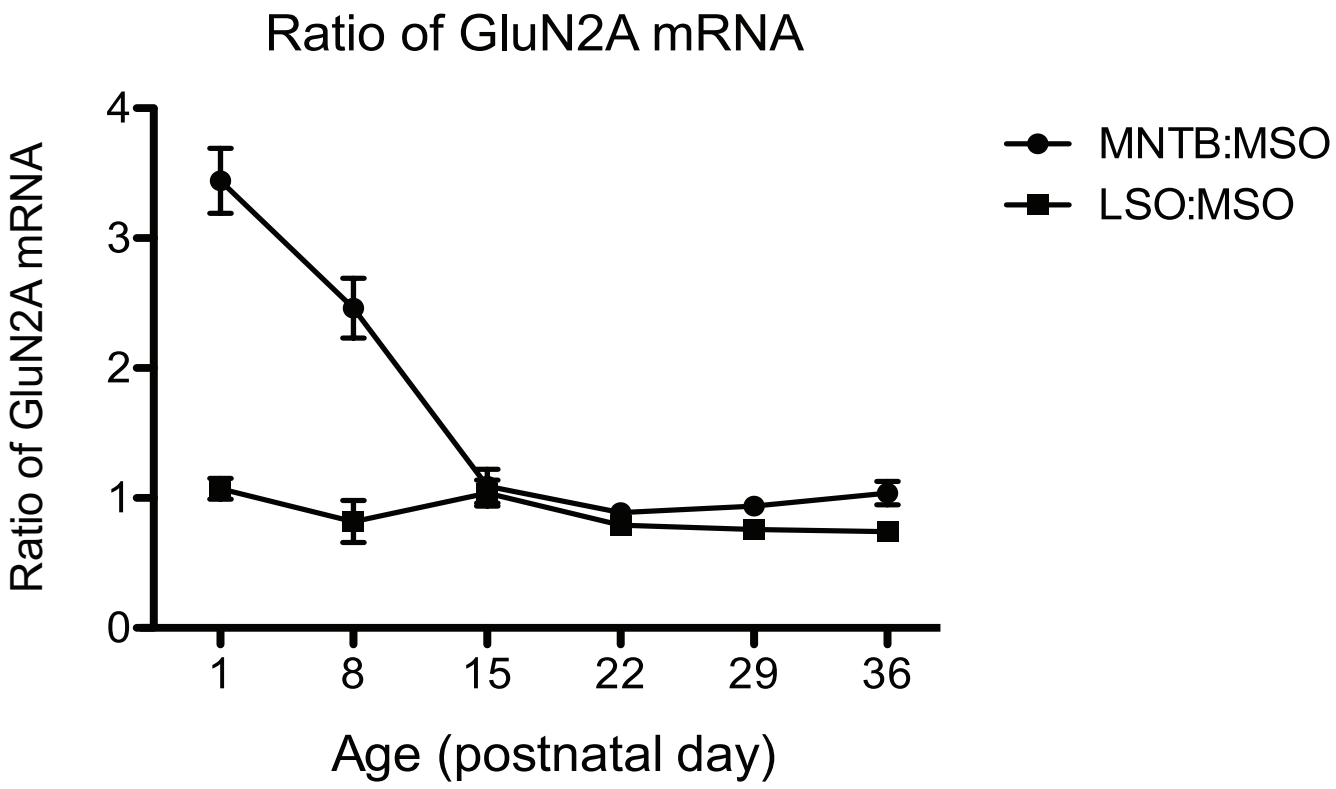

Figure 21: GluN2A mRNA expression in the MNTB and LSO normalized to GluN2A expression in the MSO. GluN2A expression in the MNTB normalized to the MSO shows a distinct expression pattern when compared to GluN2A expression normalized to the MSO.

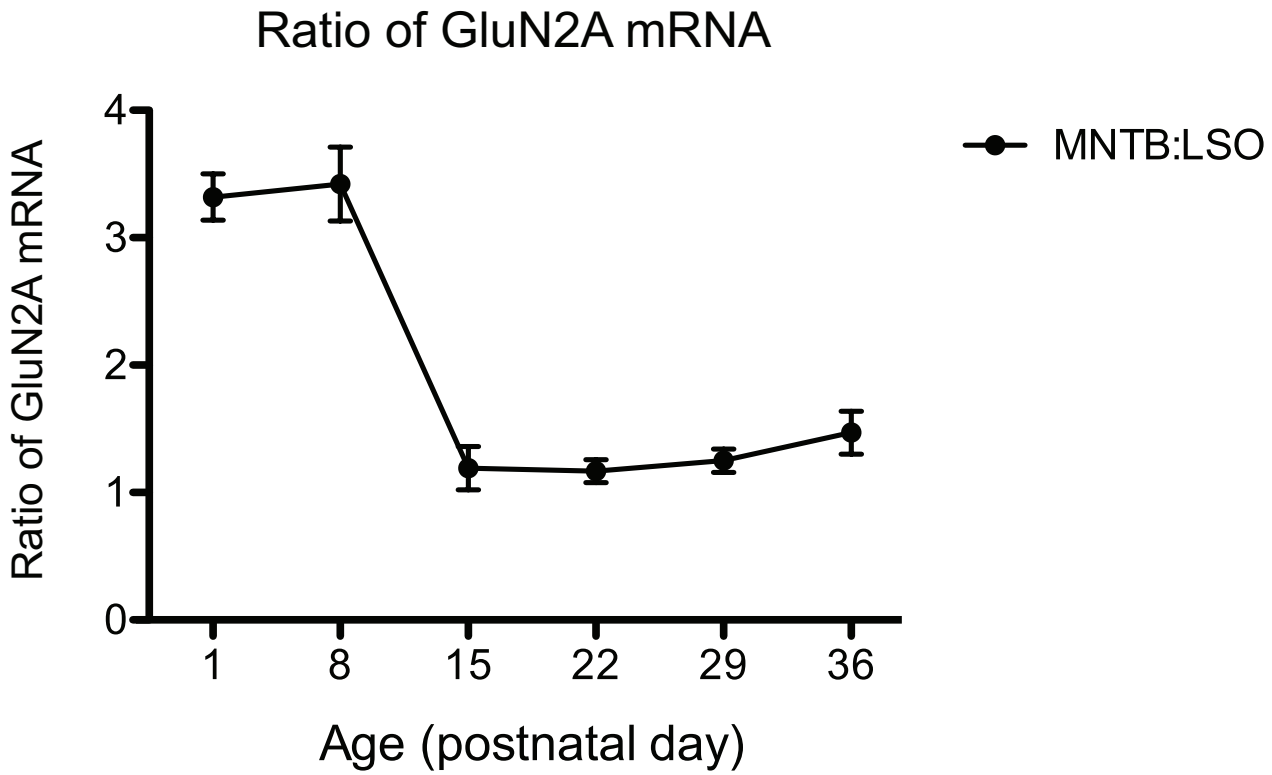

Figure 22: GluN2A mRNA expression in the MNTB normalized to GluN2A expression in the LSO. GluN2A expression in the MNTB normalized to the LSO shows a similar trend as seen with GluN2A expression in the MNTB normalized to the MSO.

5. Discussion

I examined the developmental mRNA expression of the NMDA receptor subunits, GluN1, GluN2A and GluN2B, in the LSO, MSO and MNTB during postnatal development. The auditory brainstem matures between P16 and P30, depending on the structure and parameter examined (Sanes & Rubel, 1988). MNTB-LSO connections undergo an early period of functional synaptic refinement (Kim & Kandler, 2003; Kim & Kandler, 2010) followed by a period of anatomical refinement after hearing onset (Kandler & Friauf, 1993). Here, we found that major changes in mRNA expression levels of GluN1, GluN2A and GluN2B were complete by the end of the third postnatal week, which supports the idea that these structures reach a mature state by this time.

The findings of this study are mostly consistent with the *in-situ* hybridization and immunocytochemistry study by Sato et al. (1999) showing high expression of GluN2A and GluN2C, with low GluN2B expression in the mature LSO. Sato et al. (1999) also saw that the MNTB had higher GluN2B expression when compared to GluN2A and GluN2C expression. In contrast to these findings, by adulthood, we found low GluN2B mRNA expression in the MNTB. In the MSO, Sato et al. (1999) saw roughly equal expression patterns of all GluN2 subunits. In this study, we found that GluN1 mRNA expression decreased between birth and the third postnatal week in the LSO, MSO and MNTB. In addition, we found the highest GluN2B mRNA expression during the first postnatal week in all three

nuclei, after which levels dropped to low levels. GluN2A mRNA expression patterns were distinct in all three nuclei examined. In the LSO, GluN2A levels increased during the first two postnatal weeks, then decreased to moderate levels. In the MNTB, GluN2A levels were highest during the first postnatal week, and then declined to remain stable at moderate levels. In the MSO, GluN2A mRNA levels were lowest at birth and then increased to stabilize at moderate levels by the end of first postnatal week.

It is important to note that this study examined mRNA expression levels during postnatal development of the three NMDAR subunits. The amount of subunit mRNA that is translated into protein, and subsequently assembled into functional receptors to be expressed at the cell surface is unknown. Therefore, from this study we cannot determine the amount of functional NMDA receptors in each nucleus examined. In addition, the developmental mRNA expression patterns of GluN2C, GluN2D, GluN3A and GluN3B mRNA were not examined. This study did not examine absolute levels of transcript, thus we cannot directly compare expression levels between subunits. However, we did plot the ratios of subunit expression between nuclei in order to compare relative expression patterns of these subunits between nuclei.

The GluN1 probe did not take into account the different splice variants of the GluN1 subunit (Caroll & Zukin, 2002; Cull-Candy et al., 2004) and as such, we do not know which splice variants of the GluN1 subunit were primarily

expressed in the three nuclei. GluN1 subunits assemble with GluN2/3 subunits in the ER to form functional NMDAR channels (Caroll & Zukin, 2002; Cull-Candy et al., 2004; Okabe et al., 1999). Assembled NMDARs are then trafficked to the cell surface. The GluN2 subunits could assemble with GluN1 subunits to form diheteromers or triheteromers (Cull-Candy et al, 2004; Monyer et al., 1994). Future studies should examine protein expression levels throughout postnatal development in the SOC nuclei using immunohistochemistry or immunocytochemistry, the latter as performed by Sato et al. (1999) the mature rat SOC. Designing antibodies for postsynaptic receptors, such as the NMDAR, is difficult because the postsynaptic site consists of a dense molecular assembly and as such antibody binding is difficult (Fukaya & Watanabe, 2000). Electrophysiological experiments could also be used to determine the contribution of NMDAR-mediated EPSCs to the excitatory response in the excitatory pathways within the SOC (Case & Gillespie, 2011; Case et al., 2011; Joshi & Wang, 2002; Steinert et al., 2010). GluN2B-specific antagonists, such as ifenprodil and Ro25-6981 could be used to examine the presence of NMDARs containing the GluN2B subunit (e.g. Williams, 1993; Liu et al., 2004). The specificity of ifenprodil and Ro25-6981 in blocking GluN2B-containing NMDARs is well established, whereas, the specific action of the GluN2A-specific antagonist (NVP-AAM077) in blocking only GluN2A-containing NMDARs is controversial (Berberich et al., 2005). As such, it would be difficult to use subunit-specific pharmacology to determine the contribution of GluN2A-containing NMDARs in

the SOC. In addition, the action of all subunit-specific antagonists on triheterometric NMDARs is currently unknown (Cull-Candy et al., 2004). Nevertheless, his study was an important first step in determining which NMDAR subunits are expressed in the three main brainstem nuclei involved in sound localization.

GluN1 mRNA expression decreases with postnatal development

In all three nuclei, GluN1 mRNA levels decreased between birth and the third postnatal week. Because all functional NMDA receptors contain two GluN1 subunits (Cull-Candy et al., 2001; Ishii et al., 1993), GluN1 expression indicates overall NMDA receptor expression. Based on the decline of GluN1 mRNA expression with age, we can say that, in all three nuclei, overall NMDAR mRNA expression decreased with age. By adulthood, low to moderate levels of GluN1 mRNA remained in the LSO, MSO and MNTB. These findings are consistent with electrophysiological studies that found NMDAR-mediated EPSCs in the aVCN-MNTB pathway decreased with age (Joshi & Wang, 2002; Steinert et al., 2010). Joshi & Wang (2002) found that NMDAR-mediated EPSCs virtually disappear in MNTB neurons beyond P16, whereas, Steinert et al (2010) showed that NMDAR-mediated EPSCs were still present in the MNTB, but at low levels. Steinert and colleagues performed their recordings at physiological temperatures, and used both rats and mice whereas Joshi & Wang (2002) recorded at room temperature and only in mice. We found low levels of NMDARs by adulthood in the MNTB,

which supports the findings by Steinert et al. (2010). What role could NMDA receptor expression play in the adult auditory brainstem? As NMDAR-mediated EPSCs are longer in duration than AMPAR-mediated EPSCS, NMDAR-mediated EPSCs may help shape the excitatory synaptic response in SOC nuclei. It is not known if the adult auditory brainstem can undergo plasticity, but because NMDARs are involved in forms of plasticity in other sensory brain areas (Philpot et al., 2007), they may also be involved in adult plasticity.

GluN2B mRNA expression is highest during first postnatal week

GluN2B mRNA is highly expressed in all three nuclei during the first postnatal week of development. The GluN2B subunit is expressed at high levels during the period of functional refinement in the MNTB-LSO pathway, where the number of inputs to the LSO decreases and maintained inputs are strengthened (Kim & Kandler, 2003; Kim & Kandler 2010). The aVCN-LSO pathway undergoes a similar functional refinement during this time (Case et al., 2011). GluN2B-containing NMDARs exhibit a longer decay time when compared to GluN2A-containing NMDARs (Monyer et al., 1994; Banke & Traynelis, 2003, Erreger et al., 2005). The high mRNA expression of the GluN2B subunit present at birth, then declining after the first postnatal week, is consistent with the decrease in decay time of NMDAR-mediated EPSCs in the LSO after P9 (Case et al., 2011). Therefore, my results are consistent with prior electrophysiological experiments that show NMDAR-mediated currents declining with age in the aVCN-MNTB,

aVCN-LSO and MNTB-LSO pathways (Case & Gillespie, 2011; Case et al., 2011; Steinert et al., 2011). In addition, these findings are consistent with high GluN2B expression seen at young, developmental ages in other sensory systems (Crair & Malenka, 1995; Flint et al., 2007; Hestrin, 1992). GluN2B expression patterns between all three SOC nuclei are similar, and as such, provide support for the idea that GluN2B expression is spatially and temporally regulated by similar mechanisms.

GluN2A mRNA expression increases during postnatal development

In the LSO, GluN2A expression increased slightly during the first three postnatal weeks, then decreased to moderate levels thereafter. In the MNTB, GluN2A mRNA expression remained relatively stable at high levels during the first two postnatal weeks, and then declined to moderate levels. In the MSO, GluN2A mRNA expression levels increased during the first postnatal week, and remained stable at moderate levels thereafter. In all three nuclei, GluN2A mRNA expression levels remained stable at moderate levels by adulthood. These findings are consistent with prior studies showing higher levels of GluN2A at adult ages when compared to levels at younger ages in other sensory areas (Crair & Malenka, 1995; Flint et al., 2007; Hestrin, 1992).

Ratio of GluN2A to GluN2B increases during postnatal development

The ratio of GluN2A:GluN2B increased nearly 3-fold between P8 and P15 in both the LSO and MSO. In the MNTB, there was a 2-fold increase in the GluN2A:GluN2B ratio, but the increase occurred a week earlier in development. These results are consistent with the developmental mRNA expression patterns of GluN2A and GluN2B in the auditory cortex (Hsieh et al., 2002). The switch from GluN2B-containing NMDARs to GluN2A-containing NMDARs is thought to signal the end of critical periods of plasticity in other sensory systems (Philpot et al., 2007). The sharp increase in the ratio of GluN2A to GluN2B supports the idea that the GluN2A subunit replaces the GluN2B subunit during development, as seen in many other sensory areas (Crair & Malenka, 1995; Flint et al., 2007; Hestrin, 1992). Whether a critical period of plasticity exists in auditory brainstem nuclei is currently unknown; however, based on relative mRNA expression patterns during postnatal development, my results support the idea that the GluN2A the subunit replaces the GluN2B subunit. Notably, the increase in the GluN2A subunit in the LSO and MSO occurs while overall NMDAR expression (based on GluN1 mRNA levels) decreased. In addition, based on the ratios of GluN2A normalized to MSO in the LSO and MNTB, GluN2A appears to replace GluN2B much earlier in the MNTB than in the LSO or MSO.

The GluN2B subunit appears to decline to low levels with development in the LSO, MSO and the MNTB. As previously mentioned, these results suggest there may be a global mechanism regulating GluN2B expression in the SOC

nuclei. But GluN2A expression patterns were markedly different throughout postnatal development in the LSO, MSO and MNTB, suggesting that there may be distinct mechanisms regulating the spatial and temporal expression of the GluN2A subunit in the SOC nuclei. The LSO and MSO had similar expression patterns of GluN2A throughout postnatal development. The MNTB is different from the LSO and MSO in that it is a sign-inverting relay nucleus, receiving only one major excitatory input (Smith et al., 1991). The MNTB receives an excitatory input from globular bushy cells of the contralateral aVCN, but sends inhibitory inputs to both the LSO and MSO (Smith et al., 1991). Inhibitory inputs from the MNTB are important for computing ILDs and ITDs in the LSO and MSO, respectively (Boudreau and Tsuchitani, 1968; Caird & Klinke, 1983; Goldberg & Brown, 1969; Sanes & Rubel, 1988). Both the LSO and the MSO integrate inputs from the two ears. In the mature LSO, a single LSO neuron is excited and inhibited by the same sound frequency (Kim & Kandler, 2003; Kotak and Sanes, 1996; Sanes and Rubel, 1988). In the MSO, the inhibitory input from the MNTB is important for the fine-tuning of ITDs (Grothe & Neuweiler, 2000; Kapfer et al., 2002; Magnusson et al., 2005). Thus, the inhibitory input from the MNTB is important in the topographic precision seen in the LSO and MSO. As such, GluN2A-containing NMDARs may replace GluN2B-containing NMDARs in the MNTB earlier than the in the LSO and MSO because the inputs from the MNTB are important for the reliable computations of the LSO and MSO.

Troubleshooting issues

As previously mentioned, I had hoped to examine the postnatal developmental expression of the GluN2C and GluN2D subunits. However, creating the probes for these subunits proved to be difficult. Designing primers to create the GluN2C riboprobe was difficult due to unknown reasons. The first probe did not amplify well using PCR, and after several attempts at creating the GluN2C probe using different primers, I had further problems with the later steps of riboprobe creation. The main problem occurred during the purification of the plasmid DNA. During this process, I kept losing the GluN2C DNA. To purify the DNA, I used the phenyl/chloroform method. I added one volume of phenyl:chloroform:isoamyl (PCI) alcohol, then extracted the DNA by transferring the upper aqueous tube to a new tube. After this extraction, this process was repeated with chloroform. I discovered that this was the step in which we lost the DNA. We concluded that there must have been some contamination of the chloroform, and by removing this step; we were able to successfully purify the linearized plasmid. The next step in this process is transcribing the GluN2C mRNA with radioactive ∝-35S-UTP. For reasons still unknown, after many attempts, I was unable to successfully label this probe.

For GluN2D, I ran an *in situ* hybridization on the probe that was created in the laboratory. The radioactive signal was very low in these images, and at first I thought that I might have used the sense probe instead of the antisense probe on these tissue sections. I confirmed that we had, in fact, used the antisense probe,

but we couldn't pinpoint the reason that these GluN2D images were so light. We concluded that there must have been some technical issues with the day two *in situ* procedures. When I tried to create more plasmids containing GluN2D, I had trouble growing enough colonies with GluN2D DNA. As such, I was unable to successfully label GluN2D with ∝-35S-UTP. It is possible that, the GluN2D probe signal was too low to detect by film. As such, in future *in-situ* experiments using this probe, dipped slides may need to be used for analysis. Slides that are processed for *in-situ* hybridization are subsequently dipped in emulsion, and counter-stained to allow for quantification by grain counts.

6. References

Abraham WC & Bear MF. (1996). Metaplasticity: the plasticity of synaptic plasticity. *Trends in Neurosciences, 19*(4), 126-30.

Altschul SF, Gish W, Miller W, Myers EW, Lipman DJ. (1990). Basic local alignment search tool. *Journal of Molecular Biology, 215*, 403-10.

Balakrishnan V, Becker M, Löhrke S, Nothwang HG, Güresir E, & Friauf E. (2003). Expression and function of chloride transporters during development of inhibitory neurotransmission in the auditory brainstem. *The Journal of Neuroscience, 23*(10), 4134-45.

Banke TG & Traynelis SF. (2003). Activation of NR1/NR2B NMDA receptors. *Nature Neuroscience*, *6*(2), 144-52.

Barria A & Malinow R. (2002). Subunit-specific NMDA receptor trafficking to synapses. *Neuron*, *35*(2), 345-53.

Barria A & Malinow R. (2005). NMDA receptor subunit composition controls synaptic plasticity by regulating binding to CaMKII. *Neuron*, *48*(2), 289-301.

Becker M, Nothwang HG & Friauf E. (2003). Differential expression pattern of chloride transporters NCC, NKCC2, KCC1, KCC3, KCC4, and AE3 in the developing rat auditory brainstem. *Cell and Tissue Research*, *312*(2), 155-65.

Berberich S, Punnakkal P, Jensen V, Pawlak V, Seeburg PH, Hvalby Ø & Köhr G. (2005). Lack of NMDA receptor subtype selectivity for hippocampal long-term potentiation. *The Journal of Neuroscience, 25*(29), 6907-10.

Boudreau JC, & Tsuchitani C. (1968). Binaural interaction in the cat superior olive S segment. *Journal of Neurophysiology*, *31*(3), 442-54.

Brigman JL, Wright T, Talani G, Prasad-Mulcare S, Jinde S, Seabold GK, Mathur P, et al. (2010). Loss of GluN2B-containing NMDA receptors in CA1 hippocampus and cortex impairs long-term depression, reduces dendritic spine density, and disrupts learning. *The Journal of Neuroscience, 30*(13), 4590-600.

Caicedo A & Eybalin M. (1999). Glutamate receptor phenotypes in the auditory brainstem and mid-brain of the developing rat. *The European Journal of Neuroscience*, *11*(1), 51-74.

Caird D & Klinke R. (1983). Processing of binaural stimuli by cat superior olivary complex neurons. *Experimental Brain Research*, *52*, 385-399.

Cao JY, Qiu S, Zhang J, Wang JJ, Zhang XM, & Luo JH. (2011). Transmembrane region of N-Methyl-D-aspartate receptor (NMDAR) subunit is required for receptor subunit assembly. *The Journal of Biological Chemistry*, *286*(31), 27698-705.

Carmignoto G, & Vicini S. (1992). Activity-dependent decrease in NMDA receptor responses during development of the visual cortex. *Science*, *258*(5084), 1007-11.

Carroll RC, & Zukin RS. (2002). NMDA-receptor trafficking and targeting: implications for synaptic transmission and plasticity. *Trends in Neurosciences*, *25*(11), 571-7.

Case DT, Zhao X & Gillespie DC. (2011). Functional refinement in the projection from ventral cochlear nucleus to lateral superior olive precedes hearing onset in rats. *Public Library of Science (PloS) One*, *6*(6), e20756.

Case DT & Gillespie DC. (2011). Pre- and post-synaptic properties of glutamatergic transmission in the immature inhibitory MNTB-LSO pathway. *Journal of Neurophysiology.*

Chang EH, Kotak VC, & Sanes DH. (2003). Long-term depression of synaptic inhibition is expressed postsynaptically in the developing auditory system. *Journal of Neurophysiology*, *90*(3), 1479-88.

Crair MC & Malenka RC. (1995). A critical period for long-term potentiation at thalamocortical synapses. *Nature*, *375*(6529), 325-8.

Cull-Candy SG, Brickley S & Farrant M. (2001). NMDA receptor subunits: diversity, development and disease. *Current Opinion in Neurobiology*, *11*, 327-35.

Cull-Candy SG & Leszkiewicz DN. (2004). Role of distinct NMDA receptor subtypes at central synapses. *Science's STKE: Signal Transduction Knowledge Environment*, *255*(16), 1-9.

Ehrlich I, Löhrke S & Friauf E. (1999). Shift from depolarizing to hyperpolarizing glycine action in rat auditory neurones is due to age-dependent Cl- regulation. *The Journal of Physiology*, *520*(1), 121-37.

Erreger K, Dravid SM, Banke TG, Wyllie DJA & Traynelis SF (2005). Subunit-specific gating controls rat NR1/NR2A and NR1/NR2B NMDA channel kinetics and synaptic signaling profiles. *The Journal of Physiology*, *563*(2), 345-58.

Flint AC, Maisch US, Weishaupt JH, Kriegstein AR & Monyer H. (1997). NR2A subunit expression shortens NMDA receptor synaptic currents in developing neocortex. *The Journal of Neuroscience, 17*(7), 2469-76.

Foster KA, McLaughlin N, Edbauer D, Phillips M, Bolton A, Constantine-Paton, M & Sheng M. (2010). Distinct roles of NR2A and NR2B cytoplasmic tails in long-term potentiation. *The Journal of Neuroscience, 30*(7), 2676-85.

Gillespie DC, Kim G & Kandler K. (2005). Inhibitory synapses in the developing auditory system are glutamatergic. *Nature Neuroscience*, *8*(3), 332-8.

Goldberg JM & Brown, PB. (1969). Response of binaural neurons of dog superior olivary complex to dichotic tonal stimuli: some physiological mechanisms of sound localization. *Journal of Neurophysiology*.

Grothe B & Neuweiler G. (2000). The function of the medial superior olive in small mammals: temporal receptive fields in auditory analysis. *Journal of Comparative Physiology, 186*(5), 413-23.

Hestrin S. (1992). Developmental regulation of NMDA receptor-mediated synaptic currents at a central synapse. *Nature*, *357*, 686-89.

Hsieh CY, Chen Y, Leslie FM & Metherate R. (2002). Postnatal development of NR2A and NR2B mRNA expression in rat auditory cortex and thalamus. *Journal of the Association for Research in Otolaryngology*, *3*(4), 479-87.

Ishii T, Moriyoshi K, Sugihara H, Sakurada K, Kadotani H, Yokoi M, Akazawa C, et al. (1993). Molecular characterization of the family of the N-methyl-D-aspartate receptor subunits. *The Journal of Biological Chemistry*, *268*(4), 2836-43.

Jackson H, & Parks TN. (1982). Functional synapse elimination in the developing avian cochlear nucleus with simultaneous reduction in cochlear nerve axon branching. *The Journal of Neuroscience, 2*(12), 1736-43.

Joshi I & Wang LY. (2002). Developmental profiles of glutamate receptors and synaptic transmission at a single synapse in the mouse auditory brainstem. *The Journal of Physiology*, *540*(3), 861-73.

Kakazu Y, Akaike N, Komiyama S & Nabekura J. (1999). Regulation of intracellular chloride by cotransporters in developing lateral superior olive neurons. *The Journal of Neuroscience, 19*(8), 2843-51.

Kandler K & Friauf E. (1993). Pre- and postnatal development of efferent connections of the cochlear nucleus in the rat. *The Journal of Comparative Neurology*, *328*(2), 161-84.

Kandler K & Friauf E. (1995). Development transmission of glycinergic and glutamatergic synaptic in the auditory brainstem of perinatal rats. *The Journal of Neuroscience, 15*(10), 6890-904.

Kapfer C, Seidl AH, Schweizer H & Grothe B. (2002). Experience-dependent refinement of inhibitory inputs to auditory coincidence-detector neurons. *Nature Neuroscience*, *5*(3), 247-53.

Kim G & Kandler K. (2003). Elimination and strengthening of glycinergic/GABAergic connections during tonotopic map formation. *Nature Neuroscience*, *6*(3), 282-90.

Kim G & Kandler K. (2010). Synaptic changes underlying the strengthening of GABA/glycinergic connections in the developing lateral superior olive. *Neuroscience*, *171*(3), 924-33.

Kotak VC & Sanes DH. (1996). Developmental influence of glycinergic transmission: regulation of NMDA receptor-mediated EPSPs. *The Journal of Neuroscience, 76*(5), 1836-1843.

Kotak VC & Sanes DH. (2000). Long-lasting inhibitory synaptic depression is age- and calcium-dependent. *The Journal of Neuroscience, 20*(15), 5820-6.

Kotak VC, Korada S, Schwartz IR & Sanes DH. (1998). A developmental shift from GABAergic to glycinergic transmission in the central auditory system. *The Journal of Neuroscience, 18*(12), 4646-55.

Kullmann PHM, Ene FA & Kandler K. (2002). Glycinergic and GABAergic calcium responses in the developing lateral superior olive. *The European Journal of Neuroscience*, *15*(7), 1093-104.

Leake PA, Snyder RL & Hradek GT. (2002). Postnatal refinement of auditory nerve projections to the cochlear nucleus in cats. *The Journal of Comparative Neurology*, *448*(1), 6-27.

Leonard AS, Lim IA, Hemsworth DE, Horne MC & Hell JW. (1999). Calcium/calmodulin-dependent protein kinase II is associated with the N-methyl-D-aspartate receptor. *Proceedings of the National Academy of Sciences, 96*(6), 3239-44.

Lein ES, Hawrylycz MJ, Ao N, Ayres M, Bensinger A, Bernard A, Boe AF, Boguski MS, et al. (2007). Genome-wide atlas of gene expression in the adult mouse brain. *Nature, 445*, 168-76.

Liu L, Wong TP, Pozza MF, Lingenhoehl K, Wang Y, Sheng M, Auberson YP, et al. (2004). Role of NMDA receptor subtypes in governing the direction of hippocampal synaptic plasticity. *Science*, *304*(5673), 1021-4.

Lohmann C, Ilic V & Friauf E. (1998). Development of a topographically organized auditory network in slice culture is calcium dependent. *Journal of Neurobiology*, *34*(2), 97-112.

Lu T & Trussell LO. (2007). Development and elimination of endbulb synapses in the chick cochlear nucleus. *The Journal of Neuroscience, 27*(4), 808-17.

Magnusson AK, Kapfer C, Grothe B & Koch U. (2005). Maturation of glycinergic inhibition in the gerbil medial superior olive after hearing onset. *The Journal of Physiology*, *568*(Pt 2), 497-512.

Molea D & Rubel EW. (2003). Timing and topography of nucleus magnocellularis innervation by the cochlear ganglion. *The Journal of Comparative Neurology*, *466*(4), 577-91.

Monyer H, Burnashev N, Laurie DJ, Sakmann B & Seeburg PH. (1994). Developmental and regional expression in the rat brain and functional properties of four NMDA receptors. *Neuron*, *12*(3), 529-40.

Monyer H, Sprenger R, Schoepfer R, Herb A, Higuchi M, Lomeli H, Burnashev N, Sakmann B, Seeburg PH. (1992). Heteromeric NMDA receptors: molecular and functional distinction of subtypes. *Science*, *256*(5060), 1217-21.

Nabekura J, Katsurabayashi S, Kakazu Y, Shibata S, Matsubara A, Jinno S, Mizoguchi Y, et al. (2004). Developmental switch from GABA to glycine release in single central synaptic terminals. *Nature Neuroscience*, *7*(1), 17-23.

Noh J, Seal RP, Garver JA, Edwards RH & Kandler, K. (2010). Glutamate co-release at GABA/glycinergic synapses is crucial for the refinement of an inhibitory map. *Nature Neuroscience*, *13*(2), 232-8.

Okabe S, Miwa A & Okado H. (1999). Alternative splicing of the C-terminal domain regulates cell surface expression of the NMDA receptor NR1 subunit. *The Journal of Neuroscience, 19*(18), 7781-92.

Philpot BD, Sekhar AK, Shouval HZ & Bear MF. (2001). Visual experience and deprivation bidirectionally modify the composition and function of NMDA receptors in visual cortex. *Neuron*, *29*(1), 157-69.

Philpot BD, Espinosa JS & Bear MF. (2003). Evidence for altered NMDA receptor function as a basis for metaplasticity in visual cortex. *The Journal of Neuroscience, 23*(13), 5583-8.

Philpot BD, Cho KKA & Bear MF. (2007). Obligatory role of NR2A for metaplasticity in visual cortex. *Neuron*, *53*(4), 495-502.

Rautenberg PL, Grothe B & Felmy F. (2009). Quantification of the three-dimensional morphology of coincidence detector neurons in the medial superior olive of gerbils during late postnatal development. *The Journal of Comparative Neurology*, *517*(3), 385-96.

Rietzel HJ & Friauf E. (1998). Neuron types in the rat lateral superior olive and developmental changes in the complexity of their dendritic arbors. *The Journal of Comparative Neurology*, *390*(1), 20-40.

Rosenmund C, Stern-Bach Y, Stevens CF. (1998). The Tetrameric Structure of a Glutamate Receptor Channel. *Science*, *280*(5369), 1596-99.

Rozen S & Skaletsky H. 2000. Primer3 on the WWW for general users and for biologist programmers. *Methods in Molecullar Biology (Clifton, NJ), 132*, 365-86.

Sanes DH & Takács C. (1993). Activity-dependent refinement of inhibitory connections. *The European Journal of Neuroscience*, *5*(6), 570-4.

Sanes DH & Rubel EW. (1988). The ontogeny of inhibition superior olive and excitation in the gerbil lateral. *The Journal of Neuroscience, 8*(2), 692-700.

Sato K, Nakagawa H, Kuriyama H & Altschuler RA. (1999). Differential distribution of n-methyl-d-aspartate receptor-2 subunit messenger RNA in the rat superior olivary complex. *Science*, *89*(3), 839-853.

Sheng M, Cummings J, Roldan LA, Jan YN & Jan LY. (1994). Changing subunit composition of heteromeric NMDA receptors during development of rat cortex. *Nature*, *368*, 144-7.

Smith PH, Joris PX, Carney LH & Yin TC. (1991). Projections of physiologically characterized globular bushy cell axons from the cochlear nucleus of the cat. *The Journal of Comparative Neurology, 304*(3), 387-407.

Sobczyk A, Scheuss V & Svoboda K. (2005). NMDA receptor subunit-dependent [Ca2+] signaling in individual hippocampal dendritic spines. *The Journal of Neuroscience, 25*(26), 6037-46.

Steinert JR, Postlethwaite M, Jordan MD, Chernova T, Robinson SW & Forsythe ID. (2010). NMDAR-mediated EPSCs are maintained and accelerate in time course during maturation of mouse and rat auditory brainstem in vitro. *The Journal of Physiology, 588*(3), 447-63.

Strack S & Colbran RJ. (1998). Autophosphorylation-dependent targeting of calcium/calmodulin-dependent protein kinase II by the NR2B subunit of the N-methyl-D-aspartate receptor. *The Journal of Biological Chemistry, 273*(33), 20689-92.

Takahashi T, Feldmeyer D, Suzuki N, Onodera K, Cull-Candy SG, Sakimura K & Mishina M. (1996). Functional correlation of NMDA receptor epsilon subunits expression with the properties of single-channel and synaptic currents in the developing cerebellum. *The Journal of Neuroscience, 16*(14), 4376-82.

Tritsch NX & Bergles DE. (2010). Developmental regulation of spontaneous activity in the mammalian cochlea. *The Journal of Neuroscience, 30*(4), 1539-50.

Tritsch NX, Yi E, Gale JE, Glowatzki E & Bergles DE. (2007). The origin of spontaneous activity in the developing auditory system. *Nature*, *450*(7166), 50-5.

Werthat F, Alexandrova O, Grothe B & Koch U. (2008). Experience-dependent refinement of the inhibitory axons projecting to the medial superior olive. *Developmental Neurobiology*, *68*(13), 1454-62.

Williams, K. (1993). Ifenprodil discriminates subtypes of the N-methyl-D-aspartate receptor: selectivity and mechanisms at recombinant heteromeric receptors. *Molecular Pharmacology, 44*(4), 851-9.

Yoshimura Y, Ohmura T & Komatsu Y. (2003). Two forms of synaptic plasticity with distinct dependence on age, experience, and NMDA receptor subtype in rat visual cortex. *The Journal of Neuroscience, 23*(16), 6557-66.

Zhao JP & Constantine-Paton M. (2007). NR2A-/- mice lack long-term potentiation but retain NMDA receptor and L-type Ca2+ channel-dependent long-term depression in the juvenile superior colliculus. *The Journal of Neuroscience, 27*(50), 13649-54.

APPENDIX A

Table 2. Mean DPM values of GluN1 mRNA during the first five postnatal weeks (mean DPM ± SEM)			
Age	LSO	MNTB	MSO
P1	898.13 ± 167.04	1150.67 ± 186.25	967.94 ± 129.44
P8	781.02 ± 116.98	1445.07 ± 202.88	1116.94 ± 133.51
P15	853.82 ± 112.18	1548.88 ± 190.45	984.12 ± 131.13
P22	578.25 ± 93.68	1086.37 ± 189.92	652.91 ± 116.32
P29	439.33 ± 114.04	823.87 ± 169.24	539.13 ± 148.98
P36	373.60 ± 64.17	805.93 ± 102.00	432.40 ± 69.12

Table 3. Mean DPM values of GluN2B mRNA during the first five postnatal weeks (mean DPM ± SEM)			
Age	LSO	MNTB	MSO
P1	1021.49 ± 104.67	1069.17 ± 100.95	844.19 ± 66.66
P8	717.24 ± 60.86	721.93 ± 57.11	834.09 ± 78.64
P15	367.68 ± 14.21	383.42 ± 25.14	332.37 ± 21.78
P22	269.91 ± 9.11	270.79 ± 17.73	271.24 ± 10.10
P29	254.50 ± 16.46	244.48 ± 19.45	280.00 ± 20.10
P36	254.27 ± 13.07	277.43 ± 16.28	259.79 ± 11.39

Table 4. Mean DPM values of GluN2A mRNA during the first five postnatal weeks (mean DPM ± SEM)			
Age	LSO	MNTB	MSO
P1	102.79 ± 9.47	322.09 ± 32.15	102.25 ± 10.33
P8	133.96 ± 15.69	396.66 ± 18.94	202.75 ± 23.08
P15	204.08 ± 24.06	209.52 ± 22.76	206.62 ± 10.20
P22	135.97 ± 7.83	157.91 ± 13.55	177.45 ± 8.58
P29	145.73 ± 11.71	185.18 ± 20.84	197.36 ± 12.20
P36	138.71 ± 7.52	200.18 ± 18.78	196.96 ± 12.42

APPENDIX B

Table 5. Post-hoc Bonferroni multiple comparisons for GluN1			
LSO vs. MSO			
Age	t	P value	Summary
1	0.9688	P > 0.05	ns
8	4.662	P < 0.001	***
15	1.808	P > 0.05	ns
22	1.036	P > 0.05	ns
29	1.385	P > 0.05	ns
36	0.816	P > 0.05	ns
LSO vs. MNTB			
Age	t	P value	Summary
1	3.505	P < 0.05	*
8	9.216	P < 0.0001	****
15	9.646	P < 0.0001	****
22	7.052	P < 0.0001	****
29	5.337	P < 0.0001	****
36	6	P < 0.0001	****
MSO vs. MNTB			
Age	t	P value	Summary
1	2.536	P > 0.05	ns
8	4.554	P < 0.001	***
15	7.838	P < 0.0001	****
22	6.016	P < 0.0001	****
29	3.952	P < 0.01	**
36	5.184	P < 0.0001	****

Table 6. Post-hoc Bonferroni multiple comparisons for GluN2B			
LSO vs. MSO			
Age	t	P value	Summary
1	3.904	P < 0.01	**
8	2.573	P > 0.05	ns
15	0.7774	P > 0.05	ns
22	0.02922	P > 0.05	ns
29	0.5616	P > 0.05	ns
36	0.1213	P > 0.05	ns
LSO vs. MNTB			
Age	t	P value	Summary
1	1.05	P > 0.05	ns
8	0.1033	P > 0.05	ns
15	0.3466	P > 0.05	ns
22	0.01943	P > 0.05	ns
29	0.2207	P > 0.05	ns
36	0.5098	P > 0.05	ns
MSO vs. MNTB			
Age	t	P value	Summary
1	4.953	P < 0.0001	****
8	2.469	P > 0.05	ns
15	1.124	P > 0.05	ns
22	0.009792	P > 0.05	ns
29	0.7822	P > 0.05	ns
36	0.3884	P > 0.05	ns

Table 7. Post-hoc Bonferroni multiple comparisons for GluN2A			
LSO vs. MSO			
Age	t	P value	Summary
1	0.0263	P > 0.05	ns
8	3.371	P < 0.05	*
15	0.1246	P > 0.05	ns
22	2.033	P > 0.05	ns
29	2.53	P > 0.05	ns
36	2.855	P > 0.05	ns
LSO vs. MNTB			
Age	t	P value	Summary
1	10.75	P < 0.0001	****
8	12.87	P < 0.0001	****
15	0.2664	P > 0.05	ns
22	1.076	P > 0.05	ns
29	1.933	P > 0.05	ns
36	3.013	P > 0.05	ns
MSO vs. MNTB			
Age	t	P value	Summary
1	10.77	P < 0.0001	****
8	9.503	P < 0.0001	****
15	0.1418	P > 0.05	ns
22	0.9577	P > 0.05	ns
29	0.5971	P > 0.05	ns
36	0.1577	P > 0.05	ns